GEO-SPATIAL ASSESSMENT OF FOREST HEALTH STATUS USING UAS TECHNOLOGY IN ANOPOLI, CRETE.

ISAAC OGEDA OLIECH

February ,2019

SUPERVISORS:

Dr, Panagiotis Nyktas

Ir. L.M. van Leeuwen

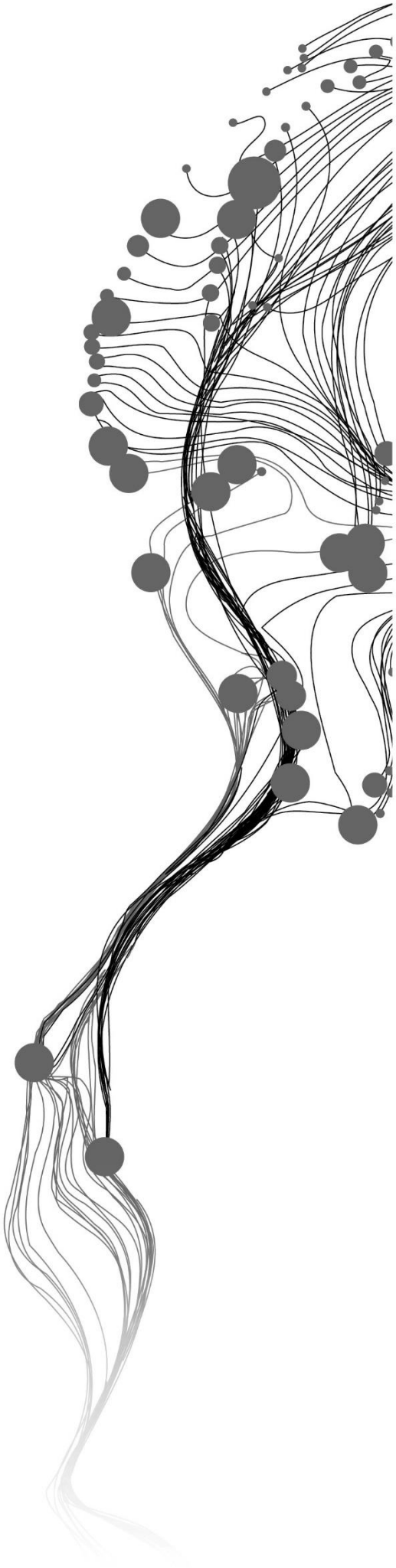

GEO-SPATIAL ASSESSMENT OF FOREST HEALTH STATUS USING UAS TECHNOLOGY IN ANOPOLI,CRETE

ISAAC OGEDA OLIECH

Enschede, The Netherlands, February,2019

Thesis submitted to the Faculty of Geo-Information Science and Earth Observation of the University of Twente in partial fulfilment of the requirements for the degree of Master of Science in Geo-information Science and Earth Observation.
Specialization: Natural Resources Management

SUPERVISORS:
dr. P. Nyktas
ir. L.M. van Leeuwen – de Leeuw

THESIS ASSESSMENT BOARD:
dr. Y. A. Hussin (Chair)
dr. Dimitris Zianis (External Examiner, Department of Forestry & Management of Natural Environment, Greece)

ABSTRACT

Despite the benefits offered by forest, forests still face numerous threats from both biotic and abiotic factors that need to be assessed. Traditional forest surveys are effective but are limited by the area of coverage. Therefore, assessing stress caused by biotic and abiotic factor using remote sensing to complement field survey is vital for maintaining healthy and productive forests over large areas. Most studies have focused on monitoring forest health using remote sensing data acquired from satellites and manned aircraft. The use of Unmanned aerial systems (UAS) offers new tools and methods for better and improved forest health assessment by offering datasets with very high spatial resolution. Data acquired from this platform can be used in unique ways and methods for monitoring forest health. In this study, we categorized the forest health into three classes, i.e., healthy moderate and severe. The primary objective was to evaluate the levels of the health status of individual trees affected by a combination of drought and pests. High spatial multi-spectral imagery was acquired using a parrot sequoia multispectral camera being mounted on the Unmanned aerial vehicle (UAV) flown over two different sites. Traditional field-based health assessments were carried out by taking into account of crown defoliation and discoloration in both sites. The crown of each tree was delineated through segmentation of the acquired multispectral images. The acquired multispectral image was used to calculate the three vegetation indices. The vegetation indices were compared in classifying the different health status of the forest while using two different non-parametric classifiers. Further, the calculated vegetation indices were used all together as one to classify forest health status. Our results showed that multi-spectral imagery obtained with UAV could be useful in categorizing different forest health status. The research found out that among the vegetation indices, soil adjusted vegetation index (SAVI) performed better than normalized difference vegetation index (NDVI) and normalized difference red-edge (NDRE) in both sites. Better results were acquired when all the vegetation indices were used at once to categorize the forest health classes. Random forest classifier slightly had a higher notch as a type of classifier over SVM across all the two sites.

Keyword: Forest health, unmanned aerial system, Pest, Vegetation indices, Classification, Assessment

ACKNOWLEDGMENTS

I would like to thank Dr. P. Nyktas for giving me an opportunity to work on this thesis, for his criticism and remarks, and his treasured advice and supervision that helped me in writing my thesis report. Also, I am very thankful to Ir. L.M. van Leeuwen for remarks, suggestions and valuable comments in my research. She was glad to help in any possible way.

I am grateful to Mr. Timothy Roberts because he was the pilot of the UAS, He was up to the task and managed to tackle the most challenges we had of flying the UAV in an area where the terrain kept flatulating. He also managed to fix some issues that arose with the sequoia camera which had delayed our data collection in the field.

Special thanks goes to the management of Samaria National park for giving us permissions to conduct flight campaign and carry out data collection in the forest. I am also grateful to them for providing us with equipment such as a sport utility vehicle (SUV) which was very helpful during the data collection, topographical maps, cameras, and binoculars. Special thanks to them for also providing us with the necessary information about our study area and sites. With their help, our work was made much easier.

Thanks to all the staff at ITC specifically from the Natural resources department for providing excellent facilities and organization of masters of geo-information science. I would like to thank Max and Sila, my friends at the university for their support and advice.

Finally, I would like to thank the Netherland fellowship program for giving me a chance to participate in the Master of Geo-information science program at ITC.

TABLE OF CONTENTS

1. INTRODUCTION 1
   1.1. Context and background 1
   1.2. Problem statement 3
2. STUDY AREA 5
   2.1. Overview of the Study Area 5
   2.2. Study Area site selection criteria in Anopoli 5
   2.3. Geology 6
   2.4. Climate 6
   2.5. Vegetation 6
   2.6. Pests in the study area 8
3. MATERIAL AND METHODS 11
   3.1. Fieldwork Materials Used 11
   3.2. Data and software used. 15
   3.3. Research Method 16
   3.4. Manual Delineation of trees 18
   3.5. Calculation of vegetation indices from the bands created 19
   3.6. Object-Based image analysis (OBIA) 20
   3.7. Segmentation procedure 21
   3.8. Segmentation accuracy assessment. 23
   3.9. Statistical Comparison of classes within the vegetation indices 24
   3.10. Separability analysis of classes within vegetation indices 24
   3.11. Classification of image objects (created segments) 24
   3.12. Accuracy assessment 25
   3.13. Post-classification analysis. 26
4. RESULTS 27
   4.1. Mosaicking images 27
   4.2. Vegetation indices 28
   4.3. Segmentation 29
   4.4. Spectral reflectance of forest health classes 31
   4.5. Statistical Comparison of classes within the vegetation indices 32
   4.6. Separability analysis of classes within vegetation indices 32
   4.7. Classification of the created segments. 33
   4.8. Accuracy assessments 35
   4.9. Post classification analysis 37
5. DISCUSSION 41
   5.1. Image Segmentation and Accuracy Assesment 41
   5.2. Separability of classes between vegetation indices 42
   5.3. Forest health classification accuracy 42
   5.4. Comparison of the two Classifiers 44
   5.5. The use of the Parrot Sequoia multispectral camera 45
   5.6. Limitation in the research 45
6. CONCLUSION AND RECOMMENDATION 46
   6.1. Conclusion. 46
   6.2. Recommendation 47

APPENDICES 54

LIST OF FIGURES

Figure 1: location of the study area, Sfakia Crete Greece. 5
Figure 2: Total monthly precipitation (blue hatched) and mean monthly air temperature (red solid line) 6
Figure 3:8 altitudinal zones of woody vegetation. altitudinal distribution of the most important tree species in the study area (A - Acer sempervirens, C Cupressus sempervirens, P - Pinus brutia, Q - Quercus cocci/era). The red oval represents the exact location. 7
Figure 4: the destruction of forest in Anopoli caused by drought and pest. 8
Figure 5: Thaumetopoea pityocampa and its destructive effects on pine trees. 8
Figure 6: (a)*Marchalina hellenica* pest (b) honeydew produced by Marchalina hellenica (c) honey production that relies on the honeydew produced (d) death of tree caused by the heavy infestation of Marchalina hellenica. 9
Figure 7:(a) *Matsucoccus josephi* pest (b, c) destructive effects to the branches and stems (d) death of a tree as a result of long-term damaging effect from *Matsucoccus josephi*. 10
Figure 8: some of the economic activity in Sfakia: left image honey being transported to the market. The right image shows goats and sheep being reared by the Sfakians. 10
Figure 9: quadcopter DJI Phantom 4, ground station and the battery used by the quadcopter 11
Figure 10: Categories of UAS(Skrzypietz 2012) 11
Figure 11: a) SEQUOIA Camera (b)The sunshine recorder(c) SEQUOIA Camera mounted on DJI Phantom 4 quadcopter. 13
Figure 12: flight plans on Universal Ground control software (site 1 right image, site 2 left image) 15
Figure 13: flow chart describing the methods applied in this study. 17
Figure 14: Segmentation process 21
Figure 15: Kappa statistics interpretation 26
Figure 16: Site 1 results of the mosaicked images (orthophoto) 27
Figure 17: Site 2 results of the mosaicked images(orthophoto) 27
Figure 18: Site1 calculated vegetation indices 28
Figure 19: Site 2 calculated vegetation indices 28
Figure 20: ESP tool for site 1 on the left and site 2 on the right. 29
Figure 21: zoomed in Multi-resolution segmentation results site1 30
Figure 22:zoomed in Multi-resolution segmentation site 2 30
Figure 23: Manually delineated(red) and the automatically generated (green) segment that used for segmentation accuracy in site1. 31
Figure 24: Spectral Reflectance of forest health status site 1 31
Figure 25: Spectral reflectance of forest health status site 2 32
Figure26: site 1; (a) RF classification using NDVI (b) SVM classification using NDVI 34
Figure27:site 1;(a) RF classification using NDRE (b) SVM classification using NDRE 34
Figure28:site 1;(a) RF classification using SAVI (b) SVM classification using SAVI 34
Figure 29: site 1;(a) RF classification using all the vegetation (b) SVM 34
Figure 30: site 2; (a)Random forest classification using NDVI (b) SVM classification using NDVI 35
Figure 31:site 2; (a)Random forest classification using NDRE (b) SVM classification using NDRE 35
Figure 32:site 2; (a) RF classification using SAVI (b) SVM classification using SAVI 35
Figure33:site2;(a) RF classification using all the vegetation(b) SVM classification using all the 35
Figure 34: Final forest health map site 1 38
Figure 35: Area in Hectares covered by each class in site 1 39
Figure 36: Final forest health Map site 2 39
Figure 37: Area in Hectares covered by each class in site 2 40

LIST OF TABLES

Table 1: Field equipment used in the study. 11
Table 2: Technical details of Parrot Sequoia camera 13
Table 3: Typical errors experienced by the handheld GNSS 14
Table 4: Expected accuracies from different kind of receivers 14
Table 5: Software used in the study 16
Table 6: Classification schema applied to study sites 18
Table 7: Segmentation accuracy in site and site 2 29
Table 8: ANOVA test in sites 1 and site 2 32
Table 9:Post hoc analysis results 32
Table 10: Separability values for the vegetation indices site 1 33
Table 11:Separability values for the vegetation indices site 2 33
Table 12: Results of error matrices site1using RF 36
Table 13: Results of error matrices site1 using SVM 36
Table 14: Results of error matrices site2 using RF 37
Table 15Results of error matrices site 2 using SVM 37

LIST OF APPENDICES

Appendix1: PIX4d software quality check report site 1 54
Appendix2: PIX4d software quality check report site 54
Appendix 3: ANOVA test within the NDRE in site 1 55
Appendix 4:Post hoc test within the NDRE in site 1 55
Appendix 5:ANOVA test within the NDVI in site1 55
Appendix 6 Post hoc test within the NDVI in site 1 55
Appendix 7:ANOVA test within the SAVI in site 1 56
Appendix 8:Post hoc test within the SAVI in site 1 56
Appendix 9:ANOVA test within the NDRE in site 2 56
Appendix 10:post hoc test within the NDRE in site 2 56
Appendix 11:ANOVA test within the NDVI in site 2 57
Appendix 12:Post hoc test within the NDVI in site 2 57
Appendix 13:ANOVA test within the SAVI in site 2 57
Appendix 14:Post hoc test within the SAVI in site 2 57
Appendix 15:Site1 Error matrix of classification NDVI Using Random forest classifier 58
Appendix 16:Site1 Error matrix of NDVI combined Using SVM 58
Appendix 17:Site1 Error matrix of NDRE combined Using Random forest classifier 58
Appendix 18:Site1 Error matrix of NDRE Using SVM 58
Appendix 19:Site2 Error matrix of SAVI Using Random forest classifier 59
Appendix 20:Site1 Error matrix of SAVI Using SVM classifier 59
Appendix 21:Site1 Error matrix of classification all vegetation indices combined Using Random forest classifier 59
Appendix 22:Site1 Error matrix of classification all vegetation indices combined Using SVM 59
Appendix 23:Site2 Error matrix of NDVI combined Using Random forest classifier 60
Appendix 24:Site2 Error matrix of NDVI combined Using SVM 60
Appendix 25:Site2 Error matrix of NDRE Using Random forest classifier 60
Appendix 26:Site2 Error matrix of NDRE Using SVM 60
Appendix 27:Site2 Error matrix of SAVI Using Random forest classifier 61
Appendix 28:Site2 Error matrix of classification all vegetation indices combined Using Random forest classifier 61
Appendix 29:Site2 Error matrix of classification all vegetation indices combined Using Random forest classifier 61
Appendix 30: Fieldwork data collection form 61

ABBREVIATIONS

ASL: Above Sea Level

CIA: Cellulose Absorption Index

GNSS: Global Navigation Satellite System

GPS: Global Positioning System

HALE: High Altitude Long Endurance

MALE: Medium Altitude Long Endurance

MTOW: Maximum Take-Off Weight

MUAV: Mini Unmanned Aerial Vehicle

NDLI: Normalized Difference Lignin Index

NDRE: Normalized Difference Red edge

NDVI: Normalized Difference Vegetation Index

NDWI: Normalized Difference Water Index

NIR: Near Infrared

RF: Random Forest

SAVI: Soil Adjusted Vegetation Indices

SDGs: Sustainable Development Goals

SVM: Support Vector Machine

UAS: Unmanned Aerial Systems

UAV: Unmanned Aerial Vehicle

VIs: Vegetation Indices

VTOL: Vertical Take-Off and Landing

1. INTRODUCTION

1.1. Context and background

Forests cover about a third of the total earth land surface (Ellison et al. 2017) and are part and parcel of the natural ecosystem. Forest are essential in providing both social economic and ecological services that are important to the well being of the human population and ensuring ecological stability around the world (Pscheidt & Deangelis 2004). Forests, for example, capture and store carbon which is very crucial in controlling carbon fluxes around the world (de Jong et al. 2018). Forest also determines downstream water supply by influencing the water movements in the watershed hydrological cycle. Most of the terrestrial biodiversity depend on the forest as their habitat. Furthermore, the forest can also be associated with Sustainable Development Goals (SDGs), for instance, more than one billion of the population around the world rely on the forest for their daily income activities that contribute their livelihood wellbeing (Chao 2012). Forest provides food for both animals and human beings, fuel, medicine, construction materials and fiber that is of use for various purposes.

However, the forest around the world faces numerous threats from drought, wind fire, air pollution, and pest infestation. Severe drought causes a reduction on net primary production and water usage which eventually leads to the death of trees, furthermore, drought causes reduced nutrient cycling and decomposition in trees which leads to the development of flammable organic material that can intensify fire outbreaks (Dale 2001). Wind causes the uprooting and breaking of tree stems and branches. Sometimes wind caused disturbances are amplified by rain, by loosening of soils that eventually causes excessive uprooting. (Gandhi et al. 2007). Massive, intense fire has a significant role in maintaining the health of a forest although sometimes they bring about excessive damages that cause the death of trees (Castello & Teale 2011). Air pollution causes the deposition of acid in the atmosphere which when mixed with rain forms acid rain (Johnson & Jacob 2010). The acid deposition by rain causes soil acidity this affects the availability of a nutrient in the soils which would eventually enable plants not to withstand factors such as drought and pest outbreaks (DeHayes et al. 1999). Also, the deposition of acid rain may cause foliar injury (Fischer et al. 2007). Pests deteriorate the health of the forest by introducing diseases to the tree which would eventually kill the trees (Food and Agriculture Organization of the United Nations 2009). Furthermore, some pests like defoliators excessively feed on the trees leaves while others bore holes in the back of the trees rendering the tree dead (Pscheidt & Deangelis 2004).

Surveillance of forest forms a major role in monitoring and effective forest health management. Studies have suggested that early assessment of trees that are facing disturbances can be a significant step in forest health management. The surveys are usually conducted by detecting symptoms or changes regarding the specific disturbances to the trees. Traditionally different methods of surveys have been used to monitor the state of forest health including detecting stress levels based on a visual examination in its early stages which at times is difficult and subjective. The use of Near-infrared spectroscopy has proven to be a challenge because these methods require extensive fieldwork for data collection and analysis which is expensive due to a huge number of workforce required and the expensive equipment required for this kind of work (Finley & Chhin 2016). Models have also been developed that gauges the forest health by using absence and presences of bird species (Nature Cconservancy 2017). Long-term forest inventories have been used in forest health monitoring since they provide valuable information about the changing trends in the forests.

However, these inventories are not sufficient enough to detect short and abrupt changes (Lausch et al. 2017). The above current methods of detecting, assessing, and monitoring forest health are sometimes not feasible, i.e., on a large-scale basis and need to be complimented.

Due to the inability of traditional ground survey methods to cover large areas, modern remote sensing methods have been suggested as the potential complement in monitoring and mapping the health status of forests. In order to fulfill the objective of forest health monitoring and mapping using remote sensing, there is a great need to know the importance of correctly knowing the data sources and the technique to be applied (Dash et al. 2017a). The choice of suitable sensors and resolution in remote sensing is normally determined by the physiological impact of the disturbances or agent affecting the forest health that can be observed based on the spectral properties of the leaves or foliage (Wulder et al. 2006). By selecting, the appropriate sensor and defining the best resolution large areas or even the whole area can be assessed with increased and improved precision (Wulder et al. 2006). One of the most common methods of conducting forest health survey using remotesensing over a large area is by aerial survey that often is also known as aerial sketch mapping. Aerial sketch mapping involves manual delineation of outbreaks and damages caused by forest disturbances. The method is conducted by a very skilled specialist aboard the airplane (Stone et al. 2012). The method is usually very accurate but is unable to detect different classes of forest disturbances outbreak and damages. Furthermore, the method itself will produce information that lacks spatial information regarding the damages reported due to lack of location measuring devices (Johnson & Ross 2008).

Acquiring digital spatial data, on the other hand, provides more advantageous capability as compared to aerial surveys. The main advantage is the spatial accuracy of the data obtained, allowing for further analysis of the digital image and providing the best level of consistency. (Dash et al. 2017a). Most studies that have been conducted have applied the use of satellite images to calculate and determine the spatial extent of damages caused by forest disturbances at a landscape and regional level using moderate spatial resolution images(5-30m)(Jonikavičius and Mozgeris 2013; Havašová et al. 2015; Meigs et al. 2011). The growing use of high-resolution satellite (<5m) in the last decade has gained popularity among researchers because of its capability to monitor and map forest health status at individual or cluster level in a particular forest stand (Adamczyk and Osberger 2015;Nicholas C. Coops et al 2006;Hart and Veblen 2015;Hicke and Logan 2009; Stone et al 2012). The high-resolution images have been reported to be much better in forest health assessment than using medium resolution (Wulder et al. 2006; Franklin et al. 2003).

Up to date the detection of forest disturbances in forestry has been a major area of focus in the field of remote sensing. However, very few studies have shown the use of satellite images(Poona & Ismail 2013), aerial survey multi-spectral data,(Leckie et al. 2004) and hyper-spectral data (Calderón et al. 2015; N C Coops et al. 2003) in mapping and assessing the impact of disturbances to forest health. This is not as compared with the field of agriculture where many studies have been conducted to assess the health status of the crops. Assessing crop health is easy because its symptoms are normally shown in the upper part of the plant, and furthermore, the area covered by crops is relatively small as compared to forests (Sankaran et al. 2010).

The use of reflectance ratio or vegetation indices (VIs) provides some of the best means in remote sensing for identifying and highlighting slight changes that occur in plants. The slight changes can be further be used to gauge the health status of the plant, or crop (Lausch et al. 2017). The vegetation indices are normally calculated on the digitally-acquired images. Vegetation indices can, therefore, be defined as the grouping of reflectance from the surface along two or more wavelength with the intention of highlighting specific characteristics of the vegetation (Tuominen et al. 2009a). Each calculated vegetation index is designed to show or highlight a particular property in a plant that could be linked to its current status (Al-Kindi et al.

2017). There are different categories of vegetation indices, and among these categories, there are different examples or type of vegetation indices. Firstly we have the carbon vegetation indices that aim at looking at the state of plants senescence. Examples of such indices include the normalized difference lignin index (NDLI) and the cellulose absorption index (CAI) (Tuominen et al. 2009a). The light efficiency index category looks at how efficient the plant is able to utilize light for photosynthesis. Examples include the photochemical reflectance index (PRI) and the structure insensitive pigment index (Barton & North 2001). The leaf pigment vegetation index provides information on stress-related pigments in the plant. Examples in this category are the anthocyanin reflectance index and the carotenoid reflectance index (Sims & Gamon 2002). Water content vegetation index provides us with the amount of water available in the canopy with less water content indicating the plant is undergoing stress. Examples of water content VIs include the moisture stress index (MSI) and the normalized difference water index (NDWI) (Tuominen et al. 2009a).`

Lastly, the most common and used category of vegetation indices are the green vegetation indices(Hart and Veblen 2015; Havašová et al. 2015; Minařík and Langhammer 2016). Green vegetation indices aim at quantifying the chlorophyll content of plants. They are the most strongly recommended category as they can detect slight variations within tree canopies; thus, one can easily distinguish different levels of forest health. Also, green vegetation indices can measure and quantify diverse aspects such as chlorophyll concentration, canopy area, and canopy structure which most of the time can indicate the level of disturbances in a forest. It can be further used to assess forest health (Tuominen et al. 2009a). Among the green vegetation indices, NDVI has popularly been used in forest health assessment studies because it has a good overall measure of greenness in vegetation (Havašová et al. 2015).On the other hand, normalized difference red edge index (NDRE.)is a broadband version of NDVI, and it is usually very sensitive to small abrupt changes in chlorophyll content as it utilizes the region along the red edge as compared to NDVI which utilizes the maximum and the minimum region of the red edge (Eitel et al. 2011). Soil adjusted vegetation index soil (SAVI), on the other hand, was established to modify NDVI so as to counter the effects of soil brightness when vegetation is low (Qi et al. 1994). The use of green vegetation indices in forest health assessment has shown acceptable accuracies especially in detecting outbreaks of forest disturbances (Meng et al. 2016; Xiao and McPherson 2005; Adamczyk and Osberger 2015), and also in mapping their damaging effects (Hart and Veblen 2015; Havašová et al. 2015; Lehmann et al. 2015).

Image classification is another technique that can be applied to acquired images so as to categorize the different levels of forest health. Classification is the grouping of pixel or objects that are similar in spectral characteristic together. There are different techniques in classification, and they include the parametric and non-parametric techniques. The parametric techniques such as maximum likelihood were traditionally being applied in classification of images, but recently the non-parametric techniques such as Classification and Regression Trees (CART), k-Nearest Neighbors (kNN), decision tree, Support Vector Machine(SVM) and Random Forests (RF) algorithms have extensively been used adopted. The most commonly used one is the random forest and the SVM, although random forest has minimally been applied in the field of forest health (Lausch et al. 2017).

1.2. Problem statement

Collecting and use of spatial digital images from satellite and the manned platforms are normally time-consuming and at times relatively costly. Due to this, images from these platforms are regarded as not suitable for forest health assessment, because they are not able to clearly detect outbreaks of forest disturbances early enough. They also do not provide the continuous monitoring of risk areas and furthermore because of their moderate resolution capability they can miss out on small patches in a forest that requires full attention (Dash et al. 2017a). Unmanned aerial vehicles (UAVs) developments in recent

years have provided new methods of acquiring very high-resolution images while at the same time offering short temporal interval images at very low cost. With the numerous advantages rendered by UAVs, still, its use in forest health assessment is scarce. For example, Näsi et al. (2015) using hyperspectral images acquired from UAV was able to classify Norway spruce forest that had been attacked by European spruce bark beetle into three classes, i.e., infested healthy and dead. The overall accuracy achieved by his classification was 76% with kappa statistics of 0.6. Lehmann et al. (2015) used UAV mounted with a compact camera to categorize five classes of forest health based on their defoliation status. The UAV was used on oak-dominated forest sites that were being attacked by the oak splendor beetle. Their classification research managed to get an overall Kappa Index of Agreement of 0.81 and 0.77 on two sites. Dash et al. (2017b) Collected multispectral images from UAV and used to identify physiological stress on tree plantation at their early stages. Their results showed that psychological stress could be early be detected using the red-edge band rather than the Near-infrared data. They further used a non-parametric method to model the physiological stress using vegetation indices and the resultant weighted kappa from their classification was 0.69.

This research, therefore, seeks to add onto the few existing studies on forest health assessment using UAV, with the application of a multispectral camera to determine the best vegetation indices that can be used to asses forest health level and best classification method.

1.2.1. General objective

To evaluate the levels of health of individual trees affected by a combination of drought and pest.

1.2.2. Specific objectives

1. To determine the vegetation index that classifies best the forest health status (NDVI, SAVI and NDRE)
2. To determine the best classifiers that classify the forest health status (RF and SVM)
3. To determine the area covered by different forest health classes.

1.2.3. Research questions

1. What accuracy is obtained when NDVI is used to classify forest health?
2. What accuracy is obtained when SAVI is used to classify forest health?
3. What accuracy is obtained when NDRE is used to classify forest health?
4. What accuracy is obtained when NDVI, SAVI and NDRE are combined to classify forest health?
5. What is the performance of the two different classifier different classifiers?
6. What is the area covered by different forest health classes?

2. STUDY AREA

2.1. Overview of the Study Area

Crete is the biggest and the most populous island in Greece and the fifth largest island in the Mediterranean Sea. Crete is divided into four regional units that are also knowns as prefectures. The regional units include Chania, Rethymno, Heraklion, and Lalitha. Heraklion is the largest and capital center of Crete with Chania coming in second. Within Chania prefectures, there are seven municipalities units which are Apokoronas, Chania, Kantanos,-Selino Kissamos, Platanias and Sfakia. Sfakia is in the southwest part of the island within Chania prefectures. Sfakia municipality was the main focus of our study area. Out of the seven villages (Patsianos, Skaloti, Agia Roumeli, Agios Ioannis, Anopoli, Askifou, Asfendou, Imbros, Chora Sfakion) in Sfakia, Anopoli was selected to be the location where the data collection was going to be carried out. Anopoli is located between latitude 35^{0} 14' 28"- 35^{0} 13' 46" and longitude 24^{0} 06' 02"- 24^{0} 00' 41"within the island with the altitude of 900m above sea level (ASL).

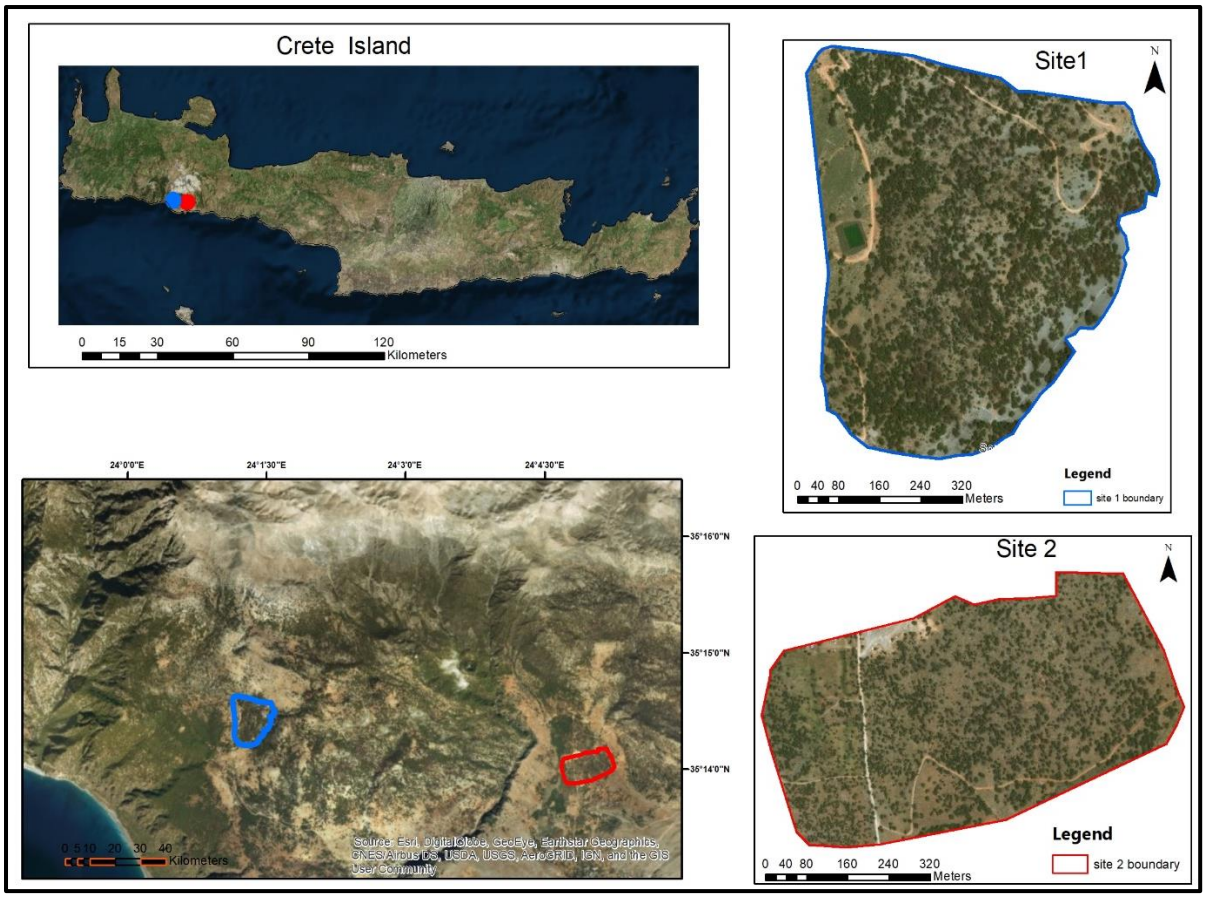

Figure 1: location of the study area, Sfakia Crete Greece.

2.2. Study Area site selection criteria in Anopoli

In Anopoli village, the study area consisted of two sites as shown in Figure 1. The study sites were chosen with the following ideas in mind.

2.2.1. Accessibility

The limited budget and time available made the study to consider the accessibility of the study site. The chosen accessible areas permitted for easy data collection using the handheld GNSS device. It also allowed the pilot to be able to watch the drone from far while still conducting its mission.

2.2.2. Composition of species

While selecting the study site, the researcher looked at the location where there was only one type of species and mixed species of coniferous trees. Site 1 was composed of pine and cypress trees in the higher altitude while site 2 composed of only pine trees located in the lower elevation sites.

2.3. Geology

The region can be described as a rugged marble that is characterized by rock debris and karstic formations that are from the dolomite massif. The soils in the area are made up of Calcaric Lithosols and are because of erosion from hard crystalline limestones and dolomites. The soils lack organic matter, very Stoney and shallow. The calcareous scree is also abundant in the soil above 900m which is as a results limestone weathering ((Fernández-Calzado et al. 2013).

2.4. Climate

The area is in the coastal Mediterranean climate and receives an annual rainfall of745- 800mm. The study area experiences six months of summer two months of winter while the remaining four months are divided in between. During March and April which is early spring, the weather is a bit windy and rainy with temperature ranging between 14℃ to 25℃ to, May and June the temperatures ranges between 25℃ to lower thirties with short rain showers. Late June and mid-September temperatures are above thirties with no rain. Mid-September to late October the temperatures are in the high twenties degree Celsius with occasional rain showers. Late October to early January the temperatures are in between 25℃ to 16℃ to degrees Celsius with windy, cloudy, rainy and warm days. Lastly, between early January to mid-March, the rainfall is high accompanied by strong winds and with temperatures ranging from 10℃ to 20℃.(Fernández-Calzado et al. 2013).Figure 2 shows show an ombrothermic diagram that summarises the total monthly precipitation and the mean monthly temperature experienced in Anopoli between the year 2015-2018. The data used to generate the ombrothermic diagram was made available to this study by Weather station of Agios Ioannis Sfakion, Crete.

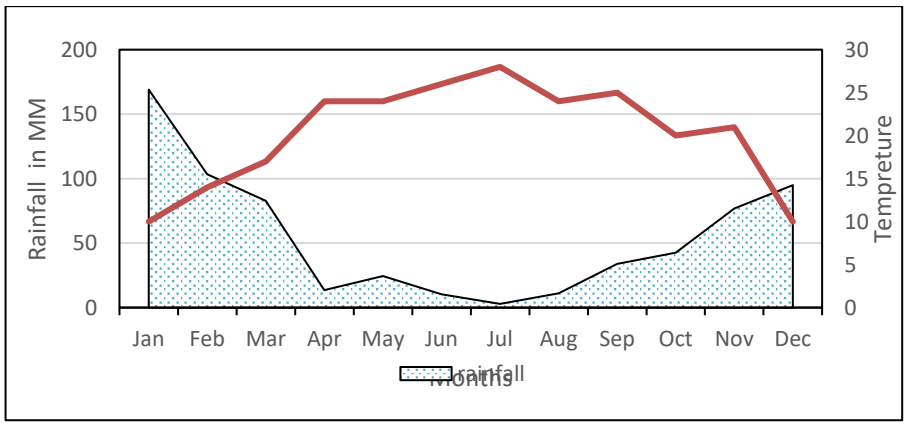

Figure 2: Total monthly precipitation (blue hatched) and mean monthly air temperature (red solid line)

2.5. Vegetation

Due to the heterogeneity of the soils and Mediterranean climate, the area is characterized by different vegetation that is either groups of spiny cushion-shaped short shrubs or low prickly scrub, for example, *Berberis cretica L.*, *Euphorbia acanthothamnos* Heldr. & Sart. ex Boiss., *Juniperus oxycedrus L. subsp oxycedrus Acantholimon androcaceum* (Jaub. & Spach) Boiss., and *Astragalus angustifolius* Lam. The

common woody tree species found in the area include Cypress, Pine, Kermes oak, Cretan maple, carob tree, Lentisc, and Myrtle (Kazakis et al. 2007).

Within the study area, there are 8 altitudinal zones of woody vegetation as shown in Figure 3. The pines (*Pinus brutia)* forms most of the lowlands between 650- 750m above sea level (ASL). Between 850 and 1150 ASL is dominated with a mixture of pine (*Pinus brutia),* and cypress (*Cupressus sempervirensis)* stands. As the altitude increases further up between 1200- 1400 the dominant species is Cyprus with a mixture of kermes oak (*Quercus coccifera)* and oriental maple *(Acer sempervirens).* As altitude progresses further up the mountain from 1450 to the timberline at 1650m, the area is characterized by pure stands of *Cupressus.* Anopoli village which is the study areas fall between 450m - 1000m ASL and this zone is composed of either pure stand of pine or a mixture of *Pinus brutia and Cupressus sempervirensis.* Figure 3 shows the zonation of the woody vegetation in Sfakia where the study area is located (red circular mark)

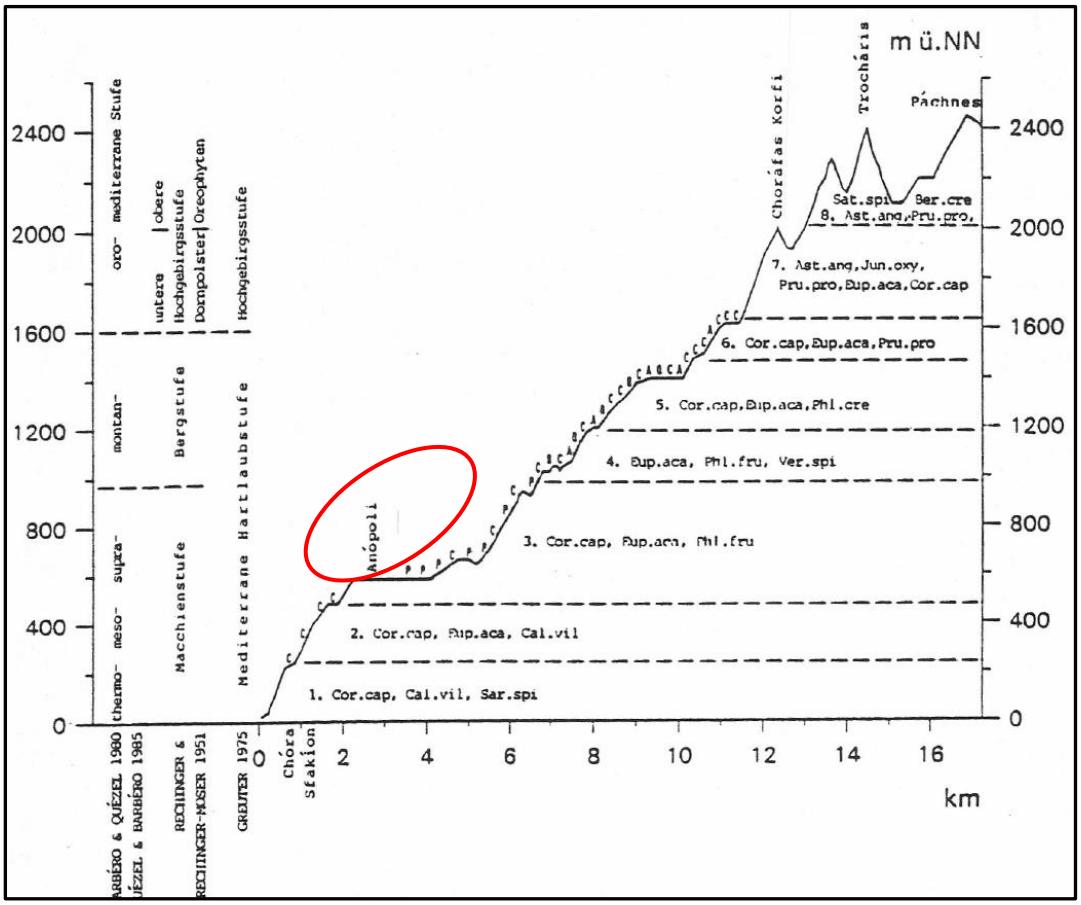

Figure 3:8 altitudinal zones of woody vegetation. altitudinal distribution of the most important tree species in the study area (A - Acer sempervirens, C *Cupressus sempervirens*, P - Pinus brutia, Q - Quercus cocciera). The red oval represents the exact location.

For this study area, site 1 has a mixture of pine and Cypress trees that are composed of both young and old trees, and the most dominant tree species was the pine tree. The crowns in the area were approximately 4 – 6 metres in diameter. The underneath of the trees in site 1 were covered with rocks bare soils and small shrubs. Site 2 was purely made of pine trees that were composed of both young and old pine trees. The crown diameter of the trees here was approximately between 2-5 meters. The underneath of the trees and the surface of the trees was covered with bare soils and very little shrubs.

2.6. Pests in the study area

The tree's health in Anopoli is damaged through a combination of drought and three pests namely *Thaumetopoea pityocampa Matsucoccus josephi and Marchalina hellenica.* The pests have caused havoc and destruction to the forest in the area. This greatly affects the net forest productivity of the area.

Figure 4: the destruction of forest in Anopoli caused by drought and pest.

Thaumetopoea pityocampa is also known as pine processionary and is a member of the moth family. *Thaumetopoea pityocampa* is one of the major causes of destruction to the Anopoli forests especially the pine trees. The pest is easily recognized by its caterpillar-like behavior. They normally form a whitish tent-like nest on pine trees leaves. The larvae of the species feeds on the pine trees causing defoliation on the entire trees leading to diebacks that leads to the eventual death of the pine trees (Hódar et al. 2003).

Figure 5: Thaumetopoea pityocampa and its destructive effects on pine trees.

Honey farmers in Greece were encouraged to introduce *Marchalina hellenica* into the pine forest in order to be able to increase their honey production. *Marchalina hellenica* is a sap-feeding insect that produces a substantial amount of honeydew. The honeydew produced is a great source of food to the bees. Studies have shown that 60% of the honey produced in Greece comes from the pine trees *that habitat of Marchalina hellenica. Marchalina hellenica* is said to be the major source of pine mortality in Greece. The pest could be found on the lower parts of the trees including the nests of the main trunks exposed roots and branches. A big population of *Marchalina hellenica* in a tree causes gradual desiccation and diebacks that could be followed by deaths of the trees. *The Marchalina hellenica* are generally located in bark crevices that are covered by a white secretion that are waxy (Mita et al. 2002).

Figure 6: (a)*Marchalina hellenica* pest (b) honeydew produced by Marchalina hellenica (c) honey production that relies on the honeydew produced (d) death of tree caused by the heavy infestation of Marchalina hellenica.

Matsucoccus josephi is the other pest that causes the mortality and destruction of forests in Anopoli. The pests feed on leaves of the branches causing shortening of the needles drying of the bud and twisting of the twigs leading to dry, sparse tree crown that would eventually cause the death of the trees. In most cases, the branches of the tree dry from the lower side to the upper side .Some of the symptoms recognized in a heavily infested pine include: tree trunks turn reddish peeling and cracking of the trunks and extravasation of huge amounts of resin drops (Mendel & Schiller 1993).

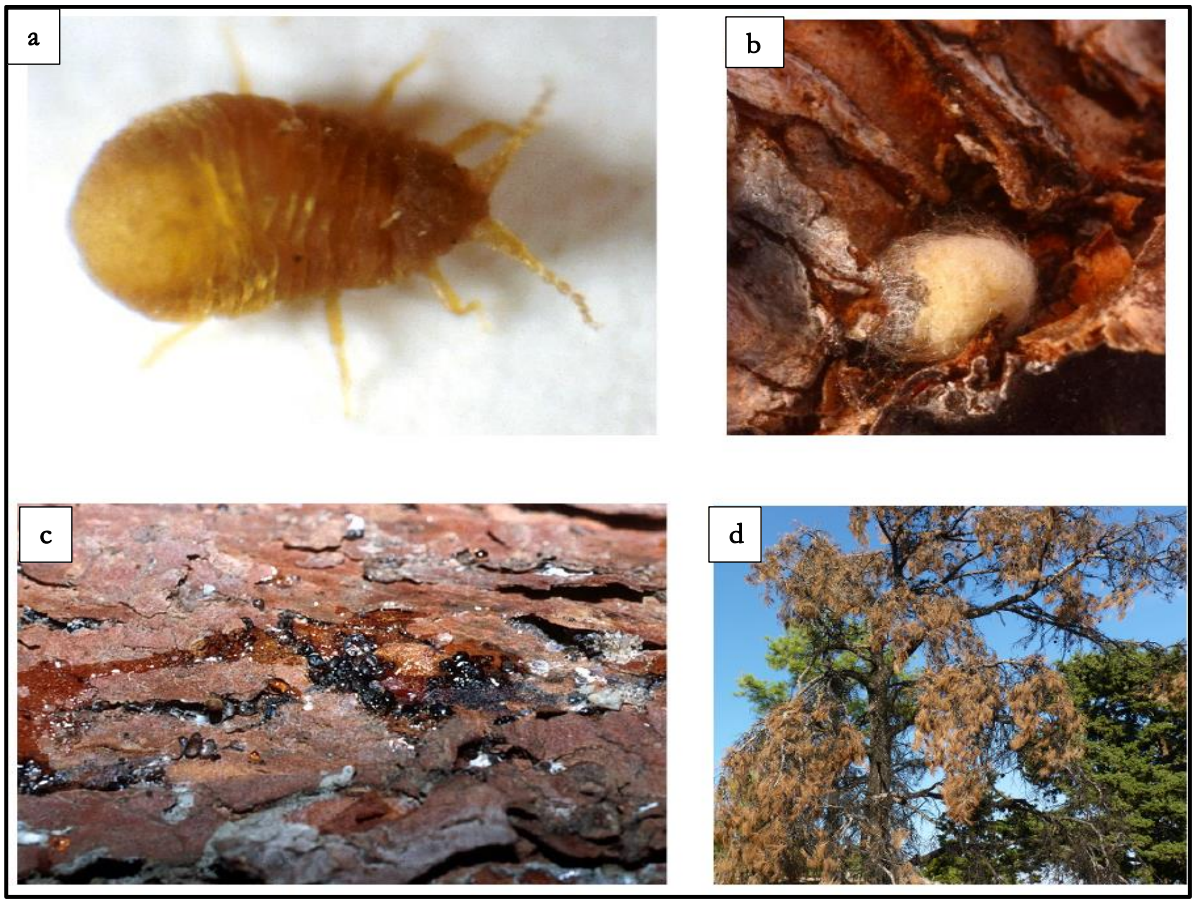

Figure 7:(a) *Matsucoccus josephi* pest (b, c) destructive effects to the branches and stems (d) death of a tree as a result of long-term damaging effect from *Matsucoccus josephi.*

2.7. Social-economic activity

The population of the study area consists of a group of people commonly referred to as Sfakians. Majority of the people are pastoralist, rearing mostly sheep and goats. Other inhabitants of the areas practice beekeeping that produces honey for sale. Cultivation of olive tree is also a common practice in the area which is the source of olive oil. The area also offers tourist destination sites with beautiful gorges, mountains for hiking beaches and beautiful scenery.

Figure 8: some of the economic activity in Sfakia: left image honey being transported to the market. The right image shows goats and sheep being reared by the Sfakians.

3. MATERIAL AND METHODS

3.1. Fieldwork Materials Used

Table 1 shows the field equipment's that were used in the field. E-Trex Garmin handheld GPS was used for navigation and recording the location of the collected samples filed data sheet was used for field observation data recording, UAV was used to fly the Sequoia camera while the Sequoia camera was used to capture multispectral images of the study area.

Table 1: Field equipment used in the study.

Field equipment	**Purpose**
UAS (Unmanned Aerial Systems)	Mounting a sequoia camera on
Datasheet	Recoding the health status during data collection
Garmin GPS	Data collection of individual trees
sequoia camera	Capturing Multispectral images.
Universal Ground control software (UGCS)	Flight planning

3.1.1. Unmanned Aerial Systems (UAS)

UAS is a system that contains three different elements namely: the ground control station where the UAV is controlled from, the aerial platform which is the flying UAV/drone and the communication element that provides the linkage between the transmitter and the receiver. Usually, the terms UAS and UAV are used interchangeably to mean the same thing, but in the real case, the UAV is the platform while the UAS entails the three components (Tang & Shao 2015).

Figure 9: quadcopter DJI Phantom 4, ground station and the battery used by the quadcopter

There are different categories of UAS systems which are generally categorized based on maximum take-off weight, flight height range in kilometers and endurance in hours as shown in Figure 10.

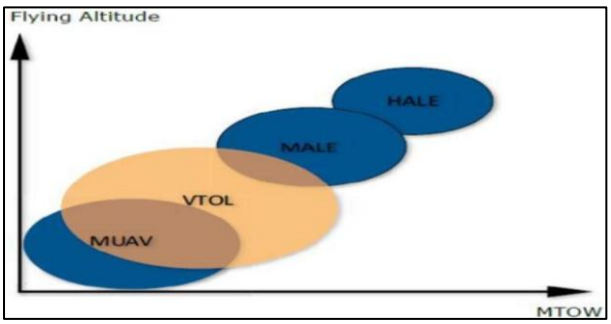

Figure 10: Categories of UAS(Skrzypietz 2012)

High altitude long endurance (HALE) and medium altitude long endurance (MALE) are regarded as a bigger and complicated system than the Mini Unmanned Aerial Vehicle (MUAV). Moreover, they are capable of carrying more payload and travel very lengthy distances (Skrzypietz 2012).

In this work, we first considered the possible pros and cons of using UAV and conventional methods of data collection. The major challenge that affects the application of UAV in forestry is relief and terrain which provides limited space for the landing and taking off the UAV. It is difficult to use some types of UAV such as the fixed wing in forestry due to the challenges mentioned above. On the other hand, the use of copters has shown more promising results due to its capability of vertical take-off and landing (VTOL). Examples of copters are the quadrotors or quadcopters that consist of disposed of rotors that are horizontally aligned (Lehmann et al. 2015).

The quadcopters have very high mobility which is enabled by their landing and take-off capabilities, precise movement and hovering capabilities (Ali & Gueaieb 2010). A research conducted on 11 different lightweight UAV with VTOL capabilities showed that the Quadcopter had been rated highly from the evaluation. The evaluation was determined based on different parameters which include miniaturization, stationary flight maneuverability, mechanics simplicity, survivability, low-speed flight, high-speed flight, and survivability (Green & Oh 2007).
This research study employed the use of the use of DJI Phantom 4 drone which is an example of a quadcopter that can be controlled from the ground station as shown in Figure 9. Using different software, we can design routes and heights to be accomplished by the UAV before flying. Furthermore, the phantom-4 is equipped with GPS and capable of performing independent missions. The DJI Phantom 4 UAV was further customized to accommodate an extra lightweight payload (Parrot Sequoia).

3.1.2. Parrot Sequoia camera

Parrot Sequoia is a small multispectral UAV camera that enables the capture of data required to monitor and respond to the health status of both agricultural and natural vegetation understudy. It has been designed in a certain way that its compatible and can be mounted on most UAV platforms. It contains four multispectral sensors, capturing data in green, red, Red-edge and Near infra-red spectral bands. At the same time, it contains a 16-megapixel RGB camera. The spectral range in the Sequoia allows one to capture both analytical non-visible data and visible image in the same flight; thus no need to re-fly the same field with different camera in capturing the data required.

A very important component of the parrot sequoia is the irradiance sensor that should be placed on top of the camera. The sensor reads the same channel of light that is being picked from the bottom and together the irradiance and the multispectral cameras are recording not only the GPS location but also the IMU data and reflection data that are then used by processing software to reconstruct the data in a very accurate way (Deng et al. 2018). Combining these technologies enables extreme precision in the task of forest health monitoring. This means that drones that are fixed with automatic control such as phantom-4 can be used to trigger the capturing sensors automatically in the sequoia making the data required simple and automated. When the Sequoia images are used with postprocessing software, it can generate index maps that are useful in vegetation monitoring. In this study, the Sequoia Camera was mounted on the Phantom-4 UAV. Figure 11 show how the parrot sequoia looks like, while Table 2 shows its technical description.

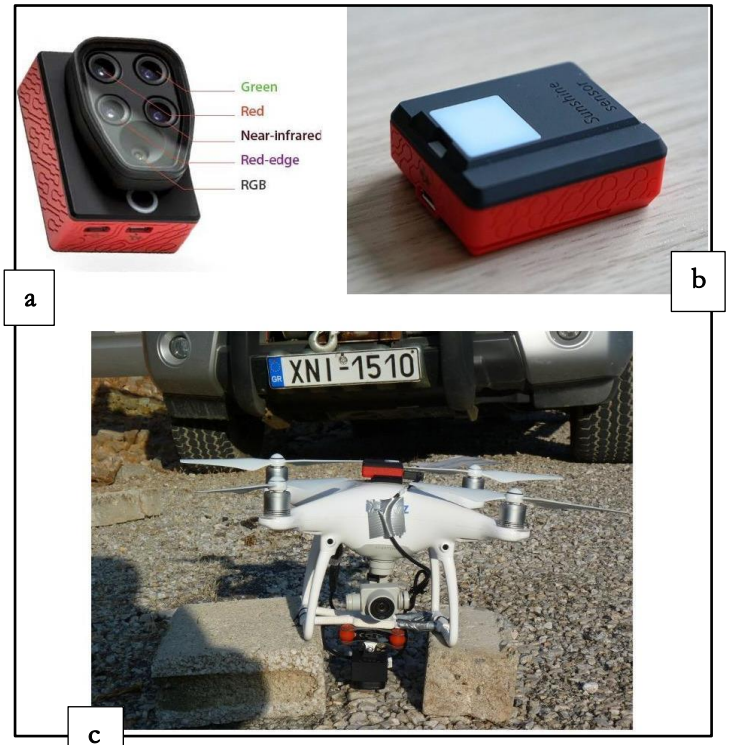

Figure 11: a) SEQUOIA Ca (b)The sunshine recorder(c) SEQUOIA Camera mounted on DJI Phantom 4 quadcopter.

Table 2: Technical details of Parrot Sequoia camera

RGB sensor (rolling shutter)	Descriptions
Pixel size	1.34 µm
Focal length	4.88 mm
Resolution	4608×3456
4 x monochrome sensors (global shutter)	Descriptions
Pixel size	3.75 µm
Focal length:	3.98 mm
Resolution:	1280 x 960
Red:	640-680 nm
Green:	530-570 nm
Red Edge:	730-740 nm
Near Infrared:	770-810 nm

3.1.3. GNSS handheld device

Satellite positioning system or global navigation satellite systems are satellite systems that are used for navigation purpose and locating areas. Examples of these satellite system include the global positioning system (GPS) Glonaas, Galileo and Beidou. Some of these systems are designed for navigational purpose around the world like GPS, while others were designed to be used at regional level like the Beidou. There are components that form the satellite-based positioning system. One of them is the user segments which entails the person using the system. Secondly, there is a control segment which controls the satellite in their

orbit and sends out indication about errors. Lastly, there are the space segments that contains a constellation of satellites. The communication among this segment works through sending of binary codes through high electromagnetic radiation known as a carrier wave (wave modulation). Different positioning system uses different codes and modulations sometimes when sending information across the segment different kinds of interference influence the time and speed at which the information is reaching the segments. This includes the accuracy of the timing device the atmosphere and redirections that is created by obstacles. To get the estimate position of a place, the recommended number of satellites should be more than or equal to three. At times the accuracy of the location might not be accurate this because of some typical error usually experienced by the positioning system(Knippers & Tempfli 2013). Examples of these errors are as shown in Table 3.

Table 3: Typical errors experienced by the handheld GNSS

Type of error	Error in Metres
Satellite clocks	2
Orbit errors	2.5
Ionosphere	5
Troposphere	0.5
Receiver noise	0.3
Multipath	?

In order to get a better accuracy of location, there are ways in which one could try and improve the positioning system. This includes eliminating random errors, use of better-quality receivers, employing the use of differential global Satellite positioning system (DGPS), and the use of a network augmenting system. Specifically, with multipath errors, one can reduce it by using the GPS on clear open skies, use of a better antenna and using an intelligent software which eliminates erroneous signals. One of the options for getting better accuracies is to use a better receiver. There are different kind of receivers, which include those that use code only like the hand-held GNSS, those that use the code and phases like the single frequency receivers and DGPS and lastly those that use code and phase on both frequencies which are known as dual frequency receivers (Knippers & Tempfli 2013). Table 4 shows the expected accuracies from different system receivers available.

Table 4: Expected accuracies from different kind of receivers

System	Accuracy in Metres
Standalone code single frequency	5-10
Standalone code dual frequency	2-5
Standalone phase	2-3
Differential code	0.5
Differential phase	0.05
Assisted network positioning	<1

For this study due to the unavailability of a more accurate receiver system we used Etrex -30 GPS which a standalone code dual frequency with an accuracy ranging from 2 to 5 meters. In the first site, the GNSS handheld Device was able to attain an accuracy of two meters while in the second site the GPS accuracy was between 3 to 5 meters.

3.1.4. Flight planning tool: Universal ground control software (UGCS)

Due to the terrain in the area, it was necessary to have planning software that would consider the issues of fluctuating terrain. In this case, the universal ground control software (UGCS) was used. UGCS software was chosen as a flight planning software because it allows the importation of Keyhole Markup Language (KML) files of the study area and automatically converts them into flight paths. It also allows planning in the terrain following mode which enables the UAV to maintain a constant altitude above the ground level. This is made possible by using the default provided SRTM or importing digital elevation model. In addition, the UGSC further offers an easy way of conducting aerial surveys by letting the selection of preinstalled camera setting or creating a new one to suit the camera on board the UAV. Based on the camera setting chosen the area scan and photogrammetry tools will automatically calculate the paths to be followed by the UAV. UGCS provides a telemetry window that can be viewed from the laptop with display information about radio link, charge level of the battery, GPS signal quality, current course heading, speed, altitude and many more which are very crucial when flying a drone in a hilly place. Finally, for large area surveys, UGCS is an effective software due to its mission planning and automation, photogrammetry geotagging tools. It enables the importation of DEM and KML files which allows for customization of the flight plans and lastly the ability to have battery change option for long routes.

In this study, the areas to be surveyed were created on Google Earth Pro. The created polygons were then saved as KML file which was later imported into the UGCS software. A combination of the default SRTM of the area and the KML files was used by the software to develop the flight plan. Additional setting such as the speed of the UAV (5m/s) the flying height (80m) and the overlaps (80%) was set and fed into the software to finalize the flight plan. The final flight plan was then sent to the UAV to conduct the mission.

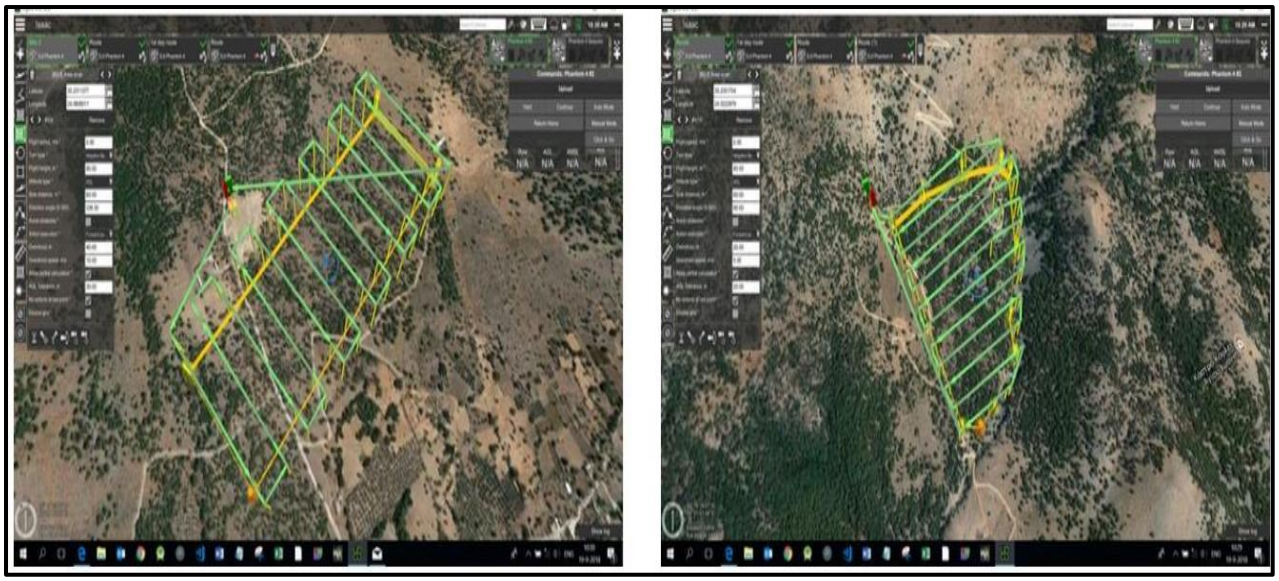

Figure 12: flight plans on Universal Ground control software (site 1 right image, site 2 left image)

3.2. Data and software used

3.2.1. UAS data

Two UAS image covering two different selected sites of the forest were used. The UAS images consisted of Four bands namely red, green Near infra-red (NIR) and the red edge. The UAS image on the first study site was acquired 15th September 2018 while the images of the second site were acquired on 18th of September

2018. The images were acquired with a Projected Coordinate System of WGS_1984_UTM_Zone_35N. Both images of Site1 and Site2 were acquired at a resolution of 8.55cm.

3.2.2. Topographical map and shapefiles

A topographical map was also used in this study. The topographical map aided in navigation and the selection of the study sites. The topographical scale boundary for the study site was 1:25000.

3.2.3. Software

The facilitation of the research was enabled using different software as shown in Table 5. Pix-4 d software was used for photogrammetry processing of UAS images. Ecognition was used for segmentation classification and accuracy assessments. Arc GIS software was used to perform some of the GIS operations and analysis. ERDAS software was used to calculate the vegetation indices and performing prepossessing of the images. Microsoft office was also used in the study.

Table 5: Software used in the study

Software	Purpose
ArcGIS	Georeferencing of orthophoto maps presentation
Pix4D	Photogrammetry processing
Erdas	Filtering and resampling of UAV images vegetation indices
Ecognition	Segmentation classification and accuracy assessments
Microsoft office	Field validation data entry and Thesis writing
SPSS	Statistical analysis

3.3. Research Method

The study applied three steps; the firsts steps included field data collection of UAV images and collection of training and validation sample. Secondly, there was the image processing part which included segmentation calculation of vegetation indices and classification. The last step involved the determination of the accuracy of the map produced through accuracy assessments technique. Figure 13 shows the flow chart of the steps.

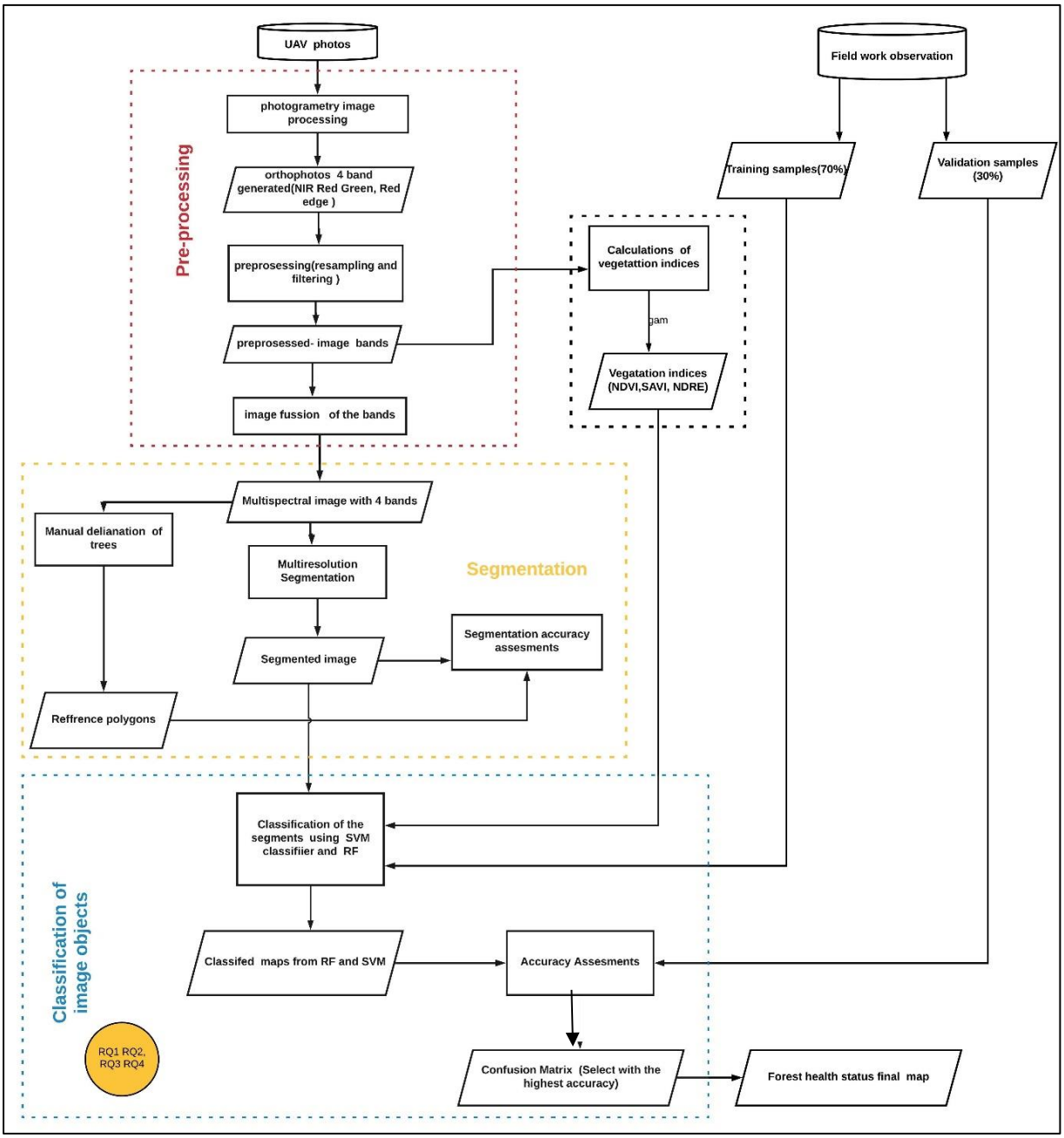

Figure 13: flow chart describing the methods applied in this study.

3.3.1. Field observations

Sample trees location representing different forest health classes was collected across the study sites to be used for training and validation in classification. Determination of the classes of data to be collected in the field had been developed as shown in appendix 30. For this case, a classification schema had to be used. The classification scheme of forest health assessment used the requirements set by the European Commission Regulation (EEC) No. 926/93 (CEC, 1993) often used to assess forest dist+urbances. The scheme used in this study was adapted to make it broader due to the cons of remote sensing methods for distinguishing detailed forest features, compared to fieldwork inventories.

Table 6: Classification schema applied to study sites

UN/ECE AND EU CLASSIFICATION SCHEMA			MODIFIED AND ADAPTED CLASSIFICATION SCHEMA		
Class	*Defoliation*	*Discoloration*	*Class*	*Defoliation*	*Discoloration*
Healthy	10%	10%	Healthy	10%	10%
Slight	10–25%	10–25%	Moderate	>10-60%	>10-60%
Moderate	25–60%	25–60%			
Severe	>60%	> 60%	Severe	>60%	>60%
Dead	100%	100%			

Total of 109 s tree samples representing three classes was collected in site 1 while a total of 125 samples were collected in site 2. 70% of the collected samples were later selected randomly used for training purposes while 30% of the data set were also selected randomly for validation purposes.

3.3.2. Mosaicking

A stationary image acquired from a stationary camera has a small Field of View (FOV). This means that it is impossible to see what is there in the surroundings. Therefore, several images need to be stitched together to form a mosaic to increase the field of view. Image mosaicking is a common and best way of obtaining a larger field of view so that the image scene can be increased. The principle behind this process is the several images that are captured as the camera moves and contain geolocation are stitched together to obtain a single large image. As the UAV mounted with camera moves, several images are captured which later are mosaiced to produce an entire scene of view. Image mosaicking addresses the most common challenge of increasing the field of view without losing spatial resolution (Huang et al. 2008). The process of image mosaicking is divided into three steps. Firstly, the features points are established and selected at each image secondly the corresponding features among the images are established also known as feature matching. Finally, the transformation of the mosaiced image is made while using points that are corresponding to create an orthophoto (Xu et al. 2016). The process of image mosaicking was carried out in PIX4D software. For site1, A total of 376 images from each multispectral camera were stitched to form the four different bands. A total of 245 images each from the multispectral camera were mosaiced for the second site to create the four band images.

3.3.3. Filtering and re-sampling of the mosaiced UAS images

In order to improve the visual interpretability of the UAV image an image enhancement technique known as image filtering had to be done. Filtering works by magnifying the small differences in the images. The process of image filtering occurs when a kernel that has weight factors is passed on the original image. The result obtained from the process is as a result of multiplication of weight factors by the digital number from the original image and addition of all the product outcome. So to be able to carry out manual delineation of trees and conduct segmentation, low pass filter was applied on the UAV images of both sites (Tolpekin & Stein 2013). Resampling of an image is the calculation of a new pixel value from an already existing pixel of an image. The images from both sites were resampled to 0.2 meters nearest neighbour technique as studies had shown that segmentation of individual trees worked best in the ranges of 0.2-0.5m resolution (Baboo & Devi 2010). The purpose of resampling using the nearest neighbor algorithm was to preserve the spectral characteristic of the trees and to make ready the image for segmentation.

3.4. Manual Delineation of trees

Manual delineation of individual trees was carried out right after the field work to aid in the determination of segmentation accuracy. The manual delineation was done on the image that was resampled and filtered. The individual trees were delineated based on specific criteria mentioned below.

1. Only the trees that were observed in the field were delineated; this was done both in site1 and in site 2.
2. A scale of 1;400 in Arc GIS was used across all the two sites for delineation purposes.
3. The diameter of the crowns was used as a reference for tree delineation.

3.5. Calculation of vegetation indices from the bands created

In remote sensing, forest health status can be assessed using features known as vegetation indices that are usually calculated from the remotely sensed dataset (Tuominen et al. 2009b). The reflectance property of the vegetation is what is used to generate these indices. The calculated vegetation indices are used to highlight a specific vegetation characteristic or feature. In this study, Greenness (chlorophyll concertation) Vegetation indices was used to map forest health status this is because of their capability to quantify diverse aspects such as chlorophyll concertation, canopy area, and canopy structure which at most time can indicate the level of forest health in a forest (Tuominen et al. 2009b). From literature reviews, three common greenness vegetation indices have been widely used in forest health mapping or monitoring. They include NDVI, SAVI, and NDRE.

3.5.1. Normalized Difference Vegetation index (NDVI)

It is one of the most commonly used vegetation indices .It measures the amount/level of greenness in the vegetation (Bannari et al. 1995). NDVI calculation is computed by the reflectance of the red band and NIR infrared as shown in equation 1:

$$\mathrm{NDVI} = \frac{(\mathrm{NIR} - \mathrm{RED})}{(\mathrm{NIR} + \mathrm{RED})}$$

Equation 1

3.5.2. Normalized Difference Red Edge Index (NDRE)

Normalized Difference Red Edge Index (NDRE) uses the reflectance along the red edge region as compared to the NDVI which employs the reflectance of maximum and minimum of the red edge region. This index is very sensitive small and abrupt chlorophyl changes(Tuominen et al. 2009a). Because of its sensitivity, NDRE has been used in a variety of forest health application such as fire damage diseases mapping bark beetle damage and drought stress. In a research conducted by Eitel et al., (2011) NDRE was able to detect stress symptoms earlier than the other vegetation indices in coniferous trees. Equation 2 shows how NDRE is computed.

$$Red\ Edge\ NDVI = \frac{NIR - Red\ Edge}{NIR + Red\ Edge}$$

Equation 2

3.5.3. Soil adjusted vegetation index (SAVI)

Soil adjusted vegetation index was made to modify the NDVI as a countermeasure for the effect of soil brightness when the vegetation is low(Bannari et al. 1995). Equation 3 below describes how this vegetation index is computed.

$$SAVI = \frac{NIR - RED}{(NIR + RED + L)} * (1 + L)$$

Equation 3

From the equation, the L value usually varies with the amount of vegetation available with L= 0 show high vegetation and L=1 no green vegetation. Generally, L= 0.5 is the default value is commonly used. In this study, the L value of 0.5 was used.

3.6. Object-Based image analysis (OBIA)

Object-based image analysis is the process of grouping or partitioning an image into a non-overlapping unit called objects or segments. The segments or objects consist of clustered pixel that shows similar characteristic either in a spatial, spectral or textural way. There are two processes that are entailed in OBIA. The first process involves performing segmentation to form segments or image object. The second process involves classifying the created segments based on different criteria such as textural properties or even custom-made properties (Blaschke 2010).

3.6.1. Segmentation

Segmentation is the process of partitioning a scene or image into non-overlapping categories or units. Segmentation is a core and fundamental process in OBIA. Therefore, it very important and crucial to establish homogeneous segments and categorize them into a particular object. (Möller et al. 2007). Segmentation techniques consist of different types, but the most common ones include; region based and edge-based segmentation (Kim et al. 2008). In this study, region-based segmentation was employed.

Region-based segmentation works in a way that it groups pixels that have pixel with similar values together while at the same time splitting pixels that are not similar. This kind of segmentation entails grouping together object to form larger objects. This can also be known as a bottom-up segmentation algorithm approach. Within the region-based techniques, there are three different types, i.e., region growing, region splitting band region merging (Pekkarinen 2004).

The region growing algorithms, groups pixel or a region into a larger region based on the criteria for growth. It begins with a set of seed points or pixel, and from the seed points, it grows the region by appending to each seed the neighbouring pixel around it that have similar properties to the seed such as specific rages colours or any other criteria such smoothness and compactness that was designated to be similar to the seed (Kamdi & Krishna 2012). Region splitting algorithms produces smaller units founded on the homogeneousness of the criterion. The smaller units are as a result of the division of larger objects. In region merging algorithm segments are merged from the primary region which can be a single pixel of the object defined (Damiand & Resch 2003).

3.6.2. Multi-resolution Segmentation

Multiresolution segmentation is an algorithm that is region based. Multiresolution segmentation was used in this study simply because it reduces the heterogeneity of a particular object while at the same time capitalizing on their homogeneity which eventually results into production of meaningful desired objects(Baatz et al. 2000). The steps mentioned below show how the multiresolution process takes place.

1. The segmentation process in one image object begins from one pixel that is also known as a seed. The seed continuously fuses with other pixels in a chain of loops up until homogeneousness is fulfilled
2. The seed will then identify the neighbouring cell that is similar, i.e., one that is the best fit and merges them together.
3. If the best fit is not achievable or not achieved, then best image object will become a candidate to be made the new seed and will start to look for its homogeneous partners again.

4. In the case where the best fit is achieved the image objects are combined in a chain of the loops. The loops will then run until further merging of the image is impossible. The process is then again repeated with other image objects.

In this study, Ecognition software was used to carry out the multi-resolution segmentation

3.6.3. Determining the multiresolution segmentation scale

The scale is crucial in defining the size of the object while undertaking the segmentation process. The presence and absence of an image object is also defined by the scale parameter. When a different scale parameter is used, the same image object will look differently (Drăguţ et al. 2010). Different scale parameters are used for different purposes for examples when classifying land cover a higher scale will be used as compared to when classifying individual trees.

The word "scale parameter" is, therefore, always used in the context of defining the highest allowable heterogeneity resultant image objects from various scale parameters. The more the image is heterogeneous the smaller the resultant image objects from the various scale, while the more homogeneous the data, the larger the image objects from various scale parameter. Varying the scale parameter allows the accommodation of desired objects. The homogeneous of the image object referred by the scale parameter is called composition of homogeneity. The composition of homogeneity relies on various factor such as colour, compactness, and weights given to layers (Drăguţ et al. 2010).

3.6.4. Estimation scale parameter (ESP) Tool

The choice of scale parameter is very important because it has a great influence on the segments produced and further can also affect the classification of segments. Within an image object, the degree of homogeneity is usually controlled by a measure known as scale parameter. For this matter, a tool known as ESP was developed that uses the local variance of an object heterogeneity in an image. With ESP tools, image objects are created iteratively at numerous scales in a bottom approach manner and the local variance of each scale is being calculated. The heterogeneity, in this case, is investigated by assessing local variance which is plotted versus the scale. The scale in which the segmentation of a scene can be done appropriately is determined by the rate of change and the local variance threshold and is always in relation to data characteristic of the image. Different studies have indicated that the use of the ESP tool has provided a speedy way of processing and producing accurate results (Drăguţ et al. 2010). In this study, the ESP tool was incorporated in ecognition software and used to determine the best scale at which the image representing two sites could be segmented in order to be able to generate individual crowns.

3.7. Segmentation procedure

A series of steps were carried out during the segmentation process this included image pre-processing multiresolution segmentation removal of non-forest area watershed transformation, morphology removal of the unwanted object and finally remaining with the desired tree crowns.

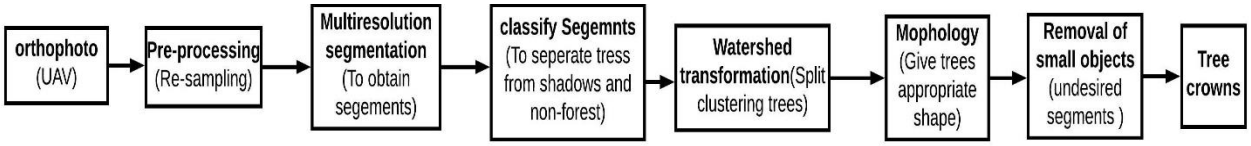

Figure 14: Segmentation process

3.7.1. Setting parameters in ESP tool

- **Scale**

Setting the scale parameter for multiresolution segmentation was done on the ESP tool. The ruleset for the ESP tool was created and added into the ecognition software. The ruleset was then executed to generate different optimum scales that were used for both sites.

- **Image Layers weighting**

Image layer weights are used to determine the band in the multispectral image that will be given priority and influence the segmentation process. For this study, the layer that was given weight was the near-infrared band with value 4 being its weight while the rest of the band were assigned the weight of 1.

- **Shape/ colour**

Shape considers the connection between the shape and colour criteria. This affects how strong the spectral values of the data will influence the homogeneity of the image object. When the value of the shape is increased the image has more uniformity spatially with less spectral uniformity vice versa. So, setting the shape field value to a lower value spectral homogeneous objects will be produced vice-versa. In this study, the shape value was set 0.8 giving little emphasis on spectral uniformity but rather spatial uniformity this is because of the different reflectance of different health status that can be in one tree.

- **Compactness**

Compactness reveals the solidity of image objects or segments to be produced. In this study, the compactness value was set to default 0.5 to produce uniform balance among objects that are compact and those that are not.

3.7.2. Masking out non-forest

The area under study was an open forest and because the UAS image was acquired at 11 AM when the shadows were noticeable in the image. Therefore, there was a need to seclude and mask out non-forest areas from the image. The values in the near-infrared image were used to separate the forested areas from non-forest areas. In both sites, pixels with NIR values, less than 0.06 were masked out as non-forest area.

3.7.3. Watershed transformation

Watershed transformation was done in ecognition software to try and tackle the situation that occurs in a natural forest which is the issue of clustering of trees in one segment. Watershed transformation splits the clustered crowns into individual crown using splitting threshold. The threshold, in this case, is usually determined based on knowledge expert of the crown.

In watershed transformation firstly, the inverted distance map is calculated. The calculation of the map is founded on the image objects border to the distance of each pixel. The calculation further converts the highest value in an original image to become the lowest value in the inverted map (Lang et al. 2007). The outcome image will resemble a watershed or a catchment. When water is put in the watershed system, the valleys in the watershed will gather water from the local minimum. The water will fill the valleys until it overspills to the next valley close to it. When the individual watersheds are close to each other and they touch one another, and the objects are split to minimize the crown clustering. In that case, when executing the watershed transformation in the forest, the clustered trees are regarded as watershed under flooding supposition. The trees are regarded as valleys that touch each other which are further separated to individual trees (L. Wang et al. 2004).

3.7.4. Morphology algorithm in eCognition software

After carrying out segmentation, the borders of the image objects created are usually not smooth. In order to smooth the image object, the morphology algorithm is applied. Two morphology operations are available

in eCognition, i.e., open image object and closed image object. In open image object, isolated pixels are removed from the image object whereas in close image object surrounding isolated pixel is added to the image. Due to small holes created or caused by shadows and difference in spectral properties, the study employed the use of close image object so that the holes could be filled. Another option provided by the morphology algorithm is the mask structuring features that also forms the basis of morphology. There are two types of mask, i.e., a circular mask and a square mask. For this circular study, masks were used in this study since the tree crowns are circular in nature.

3.7.5. Removal of undesired objects

Once the morphology process was done there seemed to be tinny objects present in the scene. The small tinny objects were objects with pixel less than 200, i.e., the crown diameter of less than 2 meters(shrubs). The small objects were removed since they were not part of trees that were being investigated. Furthermore, elongated objects that had roundness value of greater than 1.1 were also removed. The removal of elongated objects and the very small objects was performed using the remove algorithm in ecognition.

3.8. Segmentation accuracy assessment

Following the segmentation, it is always necessary to test the product of the outcome by validating the results through accuracy assessments. Accuracy assessment of the produced segments is linked to the parameter setting customization and data quality (spatial and spectral resolution). Validation of the segments or the segmentation results has to be conducted based on the geometric and topological relationship since the objects were obtained through geometric and thematic characteristics of the image. The geometric relationship is achieved by comparing the position of the object while topology is related to overlap and containment (Möller et al. 2007).

There are three ways in which segmentation accuracy can be performed or achieved using topological relationship they include: empirical goodness of fit empirical discrepancy method and analytical methods. Empirical discrepancy method works in a way that it looks at the difference between the segmented crowns and the delineated crowns (reference) to test the performance of the segmentation algorithm. The empirical goodness of fit methods assesses the algorithm functioning indirectly by evaluating the segmented images with certain quality measures established in relation to human intuition. Lastly, the analytical methods evaluates the algorithms of segmentation directly by taking into account the principles, requirements, utilities, and complexity, of the algorithms. Although it looks simple, the analytical method is unable to get all the properties of segmentation. Reasonable tests and research have shown that the empirical discrepancy methods are more effective than the analytical and goodness of fit methods assess(Zhang 1996). There are two types of errors that occur when segmentation is performed, and they include; over segmentation and under segmentation. (Liu & Xia 2010). In this case, a three-step procedure was used as proposed by (Clinton et al. 2010). The equations 4,5 and 6 below describe the procedure that was followed.

$$oversegmentatation = 1 - \frac{-(\boldsymbol{area(ADi \cap ARi)})}{area(ADi)} \quad \text{Equation 4}$$

$$undersegmentation = 1 - \frac{-(\boldsymbol{area(ADi \cap ARi)})}{area(ARi)} \quad \text{Equation 5}$$

$$\boldsymbol{D_i} = \frac{\sqrt{oversegmentatation^{\,2} + undersegmentatation^{\,2}}}{2} \quad \text{Equation 6}$$

$$Segmentattion\ accuracy = (1 - Dij) * 100 \quad \text{Equation 7}$$

Whereby:
ADi = Area of detected objects that are in a one-to-one spatial relationship with reference polygons.
ARi = Area of reference polygons
Area (ADi ∩ ARi) = Area of reference polygons that have been correctly segmented

While conducting the accuracy assessment procedure, the manually digitized polygons were used as reference polygon. A spatial join feature in Arc Map was used to identify segments that had a one to one spatial relationship with the reference polygon. Once the segment that had a spatial relationship with the reference had been established, an intersection in the Arc Map software was performed to determine the intersecting polygons. The area of the reference polygons and that of the intersects were calculated. These areas were used in equation 4 and 5 to determine over and under-segmentation. The over and under-segmentation were then used to calculate the detectable error. The overall accuracy was then calculated as shown in equation 7.

3.9. Statistical Comparison of classes within the vegetation indices

The polygons corresponding to the tree sampled in the field were used to extract vegetation indices values in Arc GIS. The extracted values were then tested for variation within the groups(healthy, moderate and severe). To do this analysis of variance (ANOVA) was used. ANOVA is a statistical test that checks if the population mean of several groups are equal or not. Therefore, the ANOVA was used for comparing three the group means for statistical significance. Furthermore, post hoc analysis was performed across all the vegetation indices using the Turkey test to see where the differences occurred between classes and to provide exact information where means are significantly different from one another. In this case before performing Anova and post hoc analysis three assumptions were made, and they include:

- The vegetation indices values were normally distributed.
- The values constitute independent random sample from the respective populations.
- The vegetation indices values had the same variance.

3.10. Separability analysis of classes within vegetation indices

After the statistical comparison of the health level of forest within the vegetation indices, a further analysis known as separability analysis was performed on the vegetation indices to find out how their values differ between classes. Separability analysis is performed with the use of the mean and the standard deviation of the field observations. The bigger the difference of the mean between classes and the smaller the standard deviation difference between the classes are, the bigger the separability (Landgrebe 2005).

$$S = (\mu 1 - \mu 2)/(\sigma 1 + \sigma 2) \qquad \text{Equation 8}$$

Where S is the separability, σ the standard deviation and μ the mean

3.11. Classification of image objects (created segments)

3.11.1. Support Vector Machine (SVM) Classifier

Support vector machine (SVM) classifier algorithm is a collection of machine learning algorithms that are commonly employed for regression analysis and classification. In classification, the main goal of SVM is to develop the best boundaries or set of boundaries that are used to differentiate the classes in the feature space. The decision boundary is commonly referred to as hyperplane or set of hyperplanes. The classification in SVM depends on which side the data falls on the hyperplane. Generally, a good hyperplane or decision

boundary is attained by the hyperplane which has the biggest distance to the closest training data of different classes. This is because when there is a larger margin, there is a lower generalization error with the classifier. In cases where the classes are not linearly separable, SVM can solve this problem by converting the data using a kernel known as radial basis function (RBF) (Raj & Sivasathya 2014).

SVM uses support vectors to classify data. These support vectors are also part of the training data input that helps in the creation of the hyperplane in the feature space. One major advantage of using the SVM algorithm is that the method has the lowest expected likelihood of generalization errors (Stephens & Diesing 2014). In this study, the SVM algorithm was implemented by developing a ruleset in ecognition. Three vegetation indices were used independently to classify the forest health status. Subsequently, the three vegetation indices were combined to see the effect of their combination in the classification of forest health.

3.11.2. Random forest Classifier

Random forest is a technique that entails a collection of many randomly developed classification trees. During the development of the random trees, two elements of randomness are normally introduced. First, a random bootstrap sample of the training datasets is used to develop each tree, secondly, instead of assessing all the characteristics for the best separation a random subset for of variables is tried at each separation or split of every tree. The reason behind introducing randomness in the development of the trees and averaging the outcomes over many trees is that the result would be lesser subjected to random variation in the training data and will have improved capability for generalizing pattern (Lausch et al. 2017). The prediction from random forest is generated for the observed data values by using the most popular class of each tree. Samples that do not constitute the bootstrap samples for the individual trees are called out of bags (OBB) sample. The OBB is used to develop cross-validated estimation error for the forest. Secondly, OBB is also used to determine the degree of feature importance. This occurs by shifting random value of input features and looking at how big the predictor error of the OBB samples intensifies (Raj & Sivasathya 2014).

3.11.3. Classification procedure

Classification of image objects produced from segmentation was undertaken based on each of the vegetation indices separately. The vegetation indices were also combined as features in ecognition ad used to classify the forest health classes. The word "combined" in this study means that the vegetation indices were used all together as independent predictors in ecognition software to classify the levels of forest health.Two classifiers namely Random Forest (RF) and Support Vector Machine(SVM) were also compared for their performance. The classification was divided into three classes in line with the tree health classes identified in the field. A total of 234 samples were chosen from both sites, 70% of which were used for classification and 30% were used further to access the accuracy of the results. In Site 1, out of 109 samples 76 were used as training samples. In site two out of 125 samples, 89 were used as training samples.

3.12. Accuracy assessment

An indispensable part of classification is the assessment of its accuracy. The most common element of accuracy assessment is the overall accuracy, user accuracy, producer accuracy, and the kappa coefficient (Al-Kindi et al. 2017). In this study, the computation of these elements will be presented.

Error matrix or confusion matrix is a method used to characterize the accuracy of the image classification. Normally the confusion matrix is a table that shows the relationship between the reference image and the classified image, i.e., in developing a confusion matrix, a ground truth or validation data are needed. The validation data can be from cartographic information results of manual digitization of an image, field work, ground survey and the record that are obtained using a handheld GNSS. Other elements of accuracy

assessment can be generated from the confusion matrix, for example, overall accuracy user accuracy and producer accuracy (Lyons et al. 2018).

Overall accuracy tells us about how the proportion of the reference data that were classified or mapped correctly. The overall accuracy is normally given in percentage with 100% being perfect in which all the ground truth data were mapped and classified correctly. Producer accuracy is the accuracy of the map from the mapmaker point of view. In other words, how frequently the features found in the ground are accurately shown on the classified image or certain features in the area being classified as such. User accuracy is the accuracy of the map from the map user point of view. This explains to us how frequent the class on the map will actually be available in the area. This is also known as reliability. Both user and producer accuracy are expressed as a percentage (Lyons et al. 2018).

Kappa statistics is an agreement measurement that is calculated from the difference between the real agreements in the error matrix as shown in equation 8. The Kappa coefficient is obtained from statistical calculations and test that gauges the accuracy of the classification. Kappa statistics generally gauges and evaluates how good the classification has performed rather than just assigning of random values (Congalton 1991)

$$\hat{K} = \frac{n\sum_{i=1}^{k} n_{ii} - \sum_{i=1}^{k} n_{i+}n_{+i}}{n^2 - \sum_{i=1}^{k} n_{i+}n_{+i}}$$

(Congalton 1991). Equation 9

where n = number of samples, $\sum_{i=1}^{k} n_{ii}$ =sum of correct classified samples, = $\sum_{i=1}^{k} n_{i+}n_{+i}$ total number of samples.

Kappa statistics values range from 0 to 1 as shown in Figure 15. The ranges that characterize the kappa statistics are <0 poor chance of agreement,0.01 to 0.2 slight agreement, 0.21-0.40 fair agreement,0.41-0.60 moderate agreement, 0.61-0.80 substantial agreement, and 0.81-0.99 almost perfect agreement (Viera & Garrett 2005).

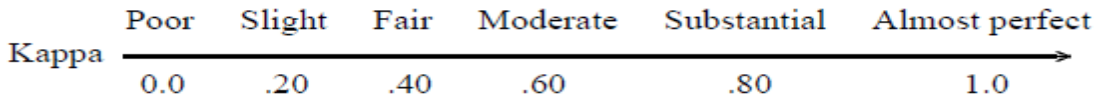

Figure 15: Kappa statistics interpretation

The accuracy assessment in this research was assessed using 30% of the collected data in the field, i.e. in site1 the classification result of the vegetation indices from both classifiers was validated using 33 observations 11 for severely infected 12 moderately infected and 10 for healthy trees. In sites two the accuracy assessment was performed using 36 observation, 13 for severe 12 for moderate and 11 for severe.

3.13. Post-classification analysis

After the comparison of random forest and SVM classified images, the best vegetation indices that classified the forest health status with higher accuracy and Kappa statistic was chosen. The selected map from the best vegetation indices went under further analysis whereby it was converted into polygons. The polygons were then used to calculate the areas covered by different forest health class . Final maps for the two sites

were then prepared. Graphs were also generated illustrating the area coverage by different forest health status class.

4. RESULTS

4.1. Mosaicking images

Mosaicking of the captured sequoia multispectral images was performed on the Pix4D software to generate the four band. The four bands were later stacked together to form a single multispectral image. The total area covered by the mosaiced images in site1 and site 2 was 44.5 and 36.3 hectares respectively with an original resolution of 8.55 cm. Figure 16 and Figure 17 shows the orthophoto created as a result of mosaicking in site 1 and site 2 respectively.

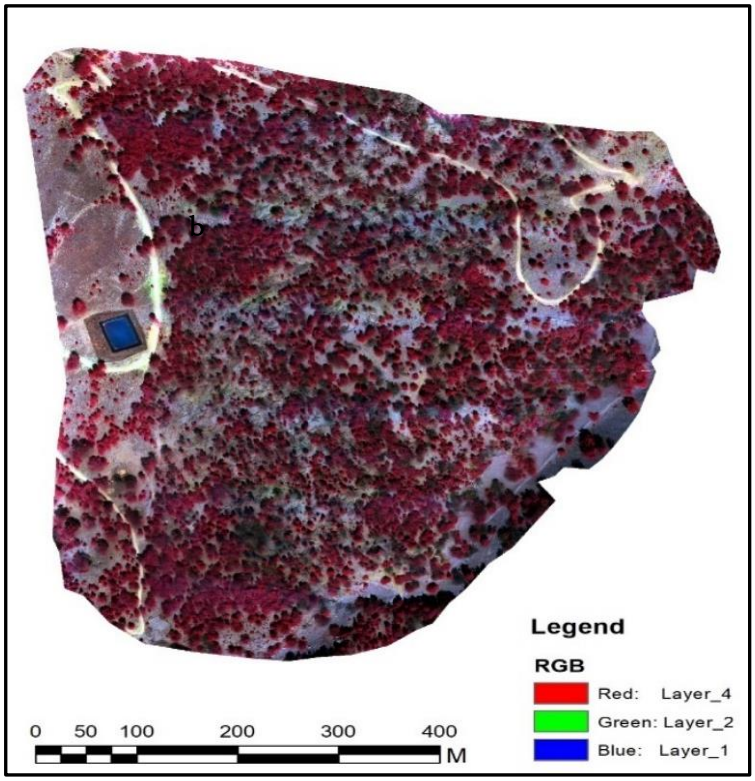

Figure 16: Site 1 results of the mosaicked images (orthophoto)

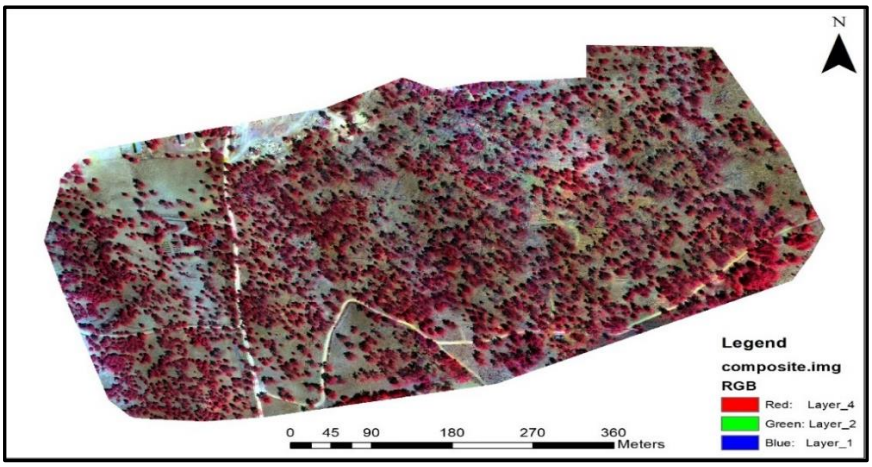

Figure 17: Site 2 results of the mosaicked images(orthophoto)

4.2. Vegetation indices

Vegetation indices were calculated using the equations 1,2,3 in ERDAS software. Figure18, and Figure 19 shows the generated vegetation indices out of the equations. From the vegetation indices maps, the brightest part which shows high values which would probably indicate healthy trees while the darkest part would represent bare ground or water bodies. Site one had NDVI values ranging from -0.63 to 0.94, SAVI values ranging from -0.23 to 0.57 and NDRE values ranging from -0.81 to 0.87. Site 2 had NDVI values ranging from 0.93 to - 0.67 SAVI values ranging from -0.38 to 0.84 and NDRE values ranging from -0.77 to -0.83.

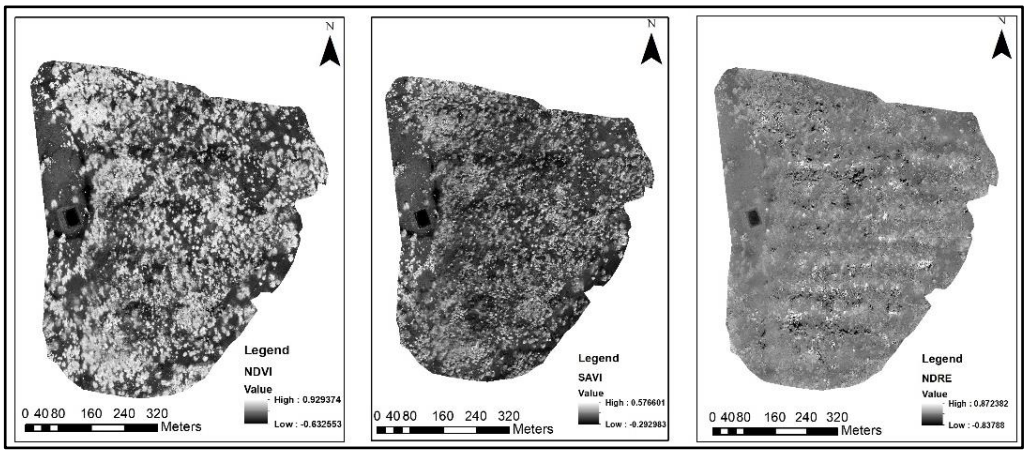

Figure 18: Site1 calculated vegetation indices

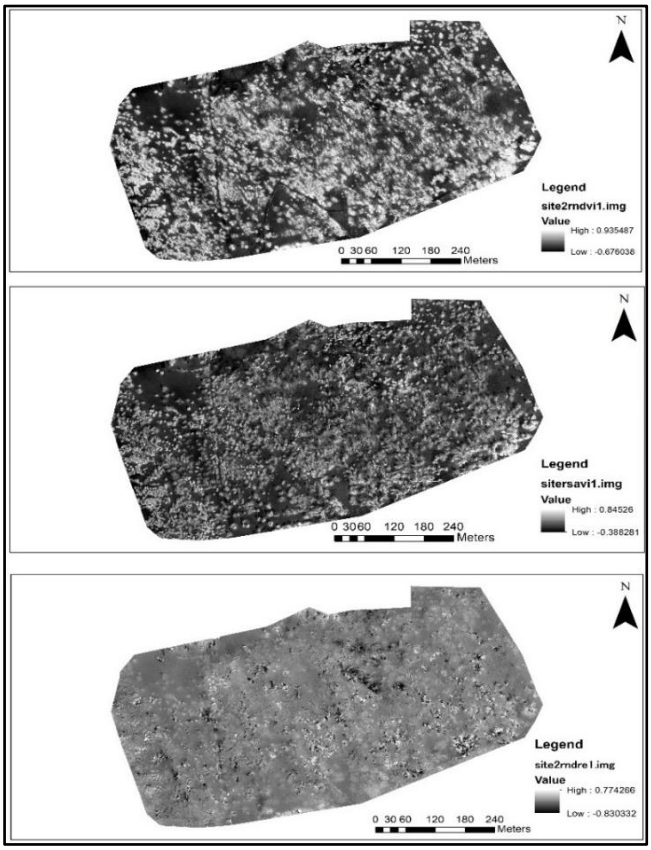

Figure 19: Site 2 calculated vegetation indices

4.3. Segmentation

Segmentation was done on both sites. In this case, the multi-resolution algorithm combined with other algorithms were applied to delineate tree crowns and also to mask out the non-forested area so as to avoid the problem of overestimating the tree crowns.

4.3.1. Estimation of Scale parameter (ESP)

ESP tool was used to determine the appropriate scale for multi-resolution segmentation. Figure 20 on the left shows the estimation of scale parameter results of the site1 image, which indicate that scale parameter 17, 19, and 21 to be suitable to segment the image. Similarly, Figure 20 on the right shows the scale parameter appropriate for site 2 image, which indicates scale parameter of 12, 14 and 20 to be suitable. These scales are the peak values of rate of change established by ESP tool in Figure 20.

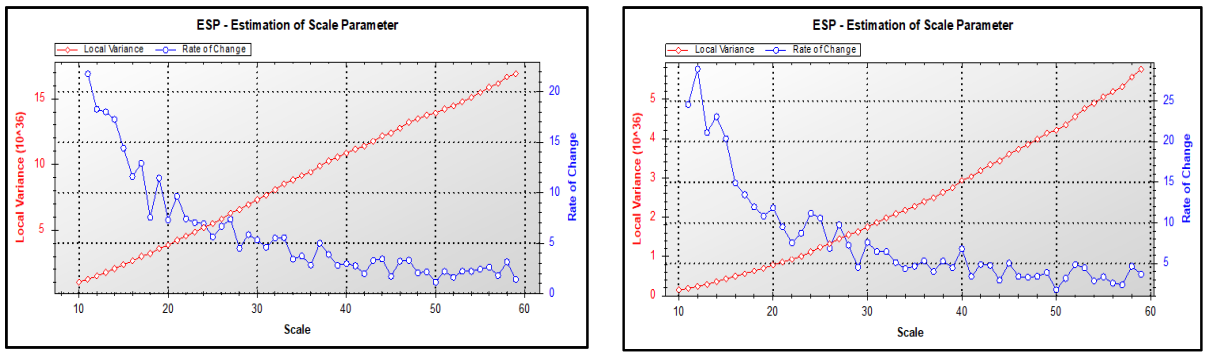

Figure 20: ESP tool for site 1 on the left and site 2 on the right.

4.3.2. Multiresolution segmentation and segmentation accuracy.

Despite using ESP tool to determine the suitable scale parameter, the three different scale in each site were tested for segmentation accuracy, and amongst them, the one with the highest accuracy was selected for further analysis. In this case, the best among the three appropriate scale parameter was 17 and 14 in site 1 and site 2 respectively. Table 7 shows the over-segmentation, under-segmentation, Dij values and accuracy assessment of the best scales in both sites.

Table 7: Segmentation accuracy in site and site 2

Segmentation Accuracy assessment	Scale 19 site 1	Scale 14 site 2
Reference area (ARi)	4415.621	4345.234
segmented area (ADi)	4202.27	6612.457
Intersection (ADi ∩ ARi)	4415.623	4396.623
Over segmentation	0.263771	0.3351
Under segmentation	-3.4E-07	-0.01183
Total detected error (Dij)	0.186514	0.236951
Accuracy 1- D	81.3%	76.3%

Multi-resolution segmentation was then carried out using the best scale parameter in each site. A total of 3215 segments were generated in site 1 while 2674 segments were generated in site 2.
Figure 21 and Figure 22 shows the final product of segmentation from both sites.

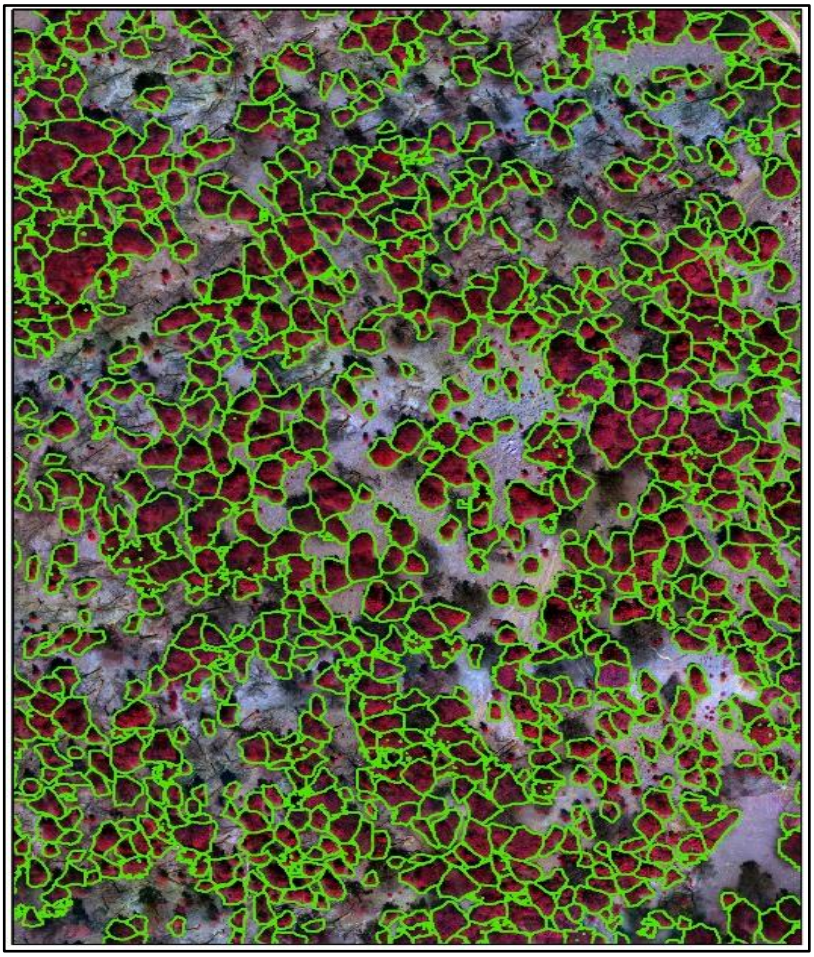

Figure 21: zoomed in Multi-resolution segmentation results site1

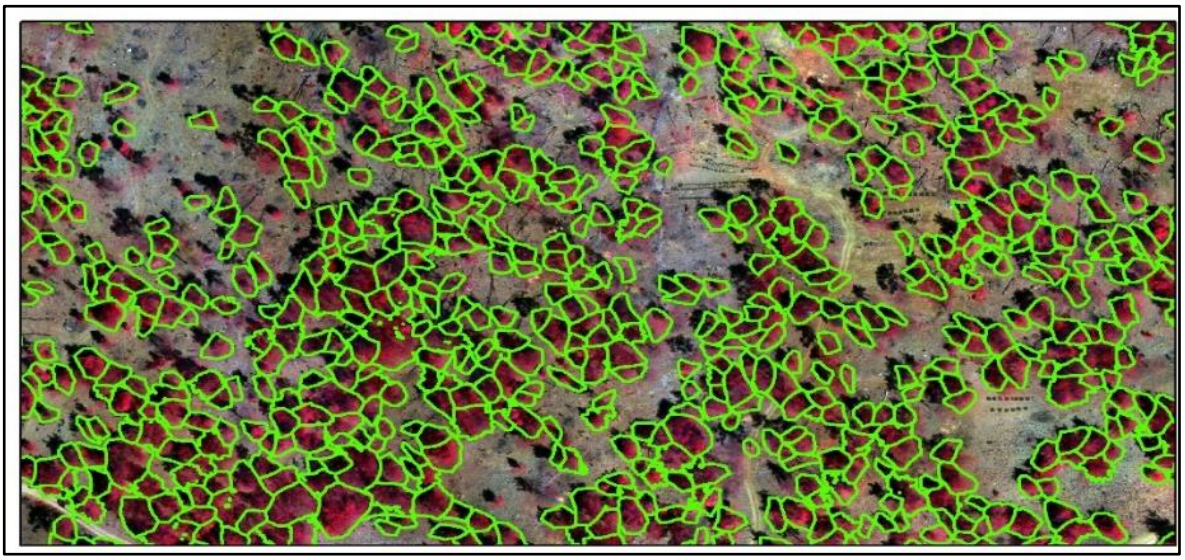

Figure 22:zoomed in Multi-resolution segmentation site 2

Figure 23 shows an example of a reference polygon that was manually delineated and the automatically generated segment polygons that were used for segmentation accuracy. The manually delineated polygons are in red while the automatically generated segments are in green color.

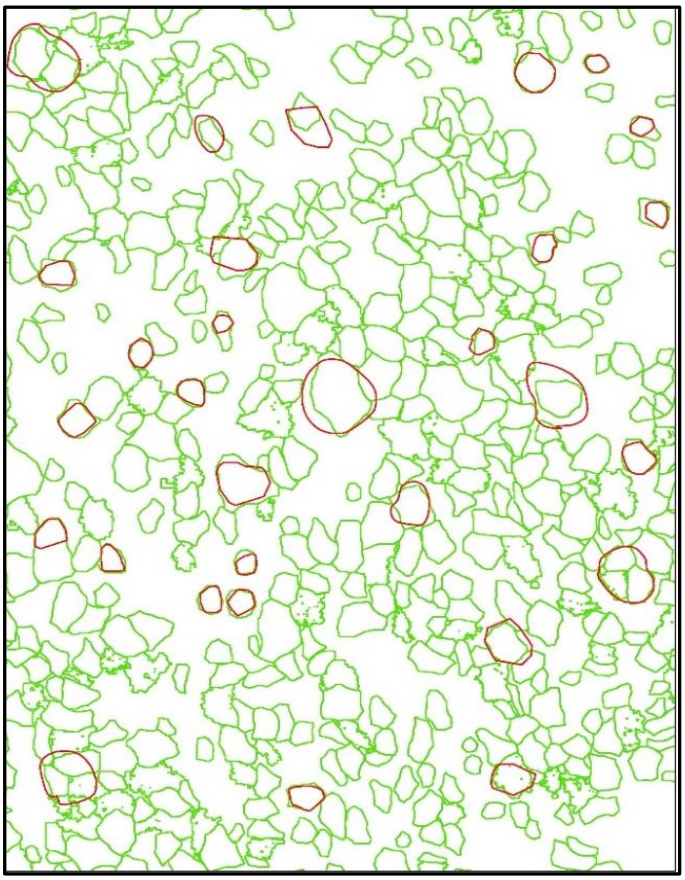

Figure 23: Manually delineated(red) and the automatically generated (green) segment that used for segmentation accuracy in site1.

4.4. Spectral reflectance of forest health classes

The spectral means reflectance values of the three forest health levels according to each band were analyzed to see how they behave in the four spectral bands. The observations made on the field were used to derive the spectral reflectance curve as seen in Figure 24 and Figure 25. The spectral reflectance in figure 24 and 25 shows the class "healthy" being very distinct from the class "moderate" and "severe "trees in the NIR region. The class severe and moderate can be seen as not very distinctive from each other.

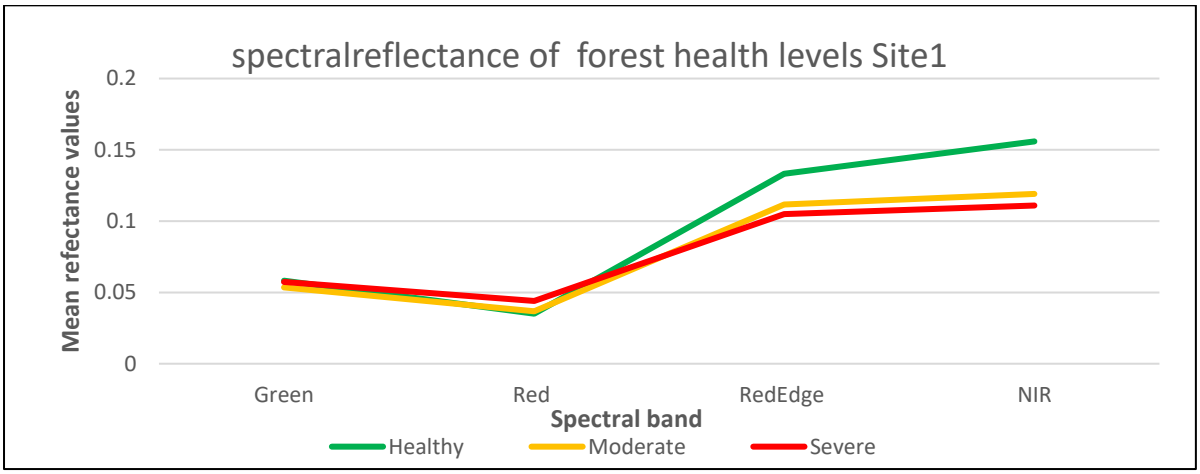

Figure 24: Spectral Reflectance of forest health status site 1

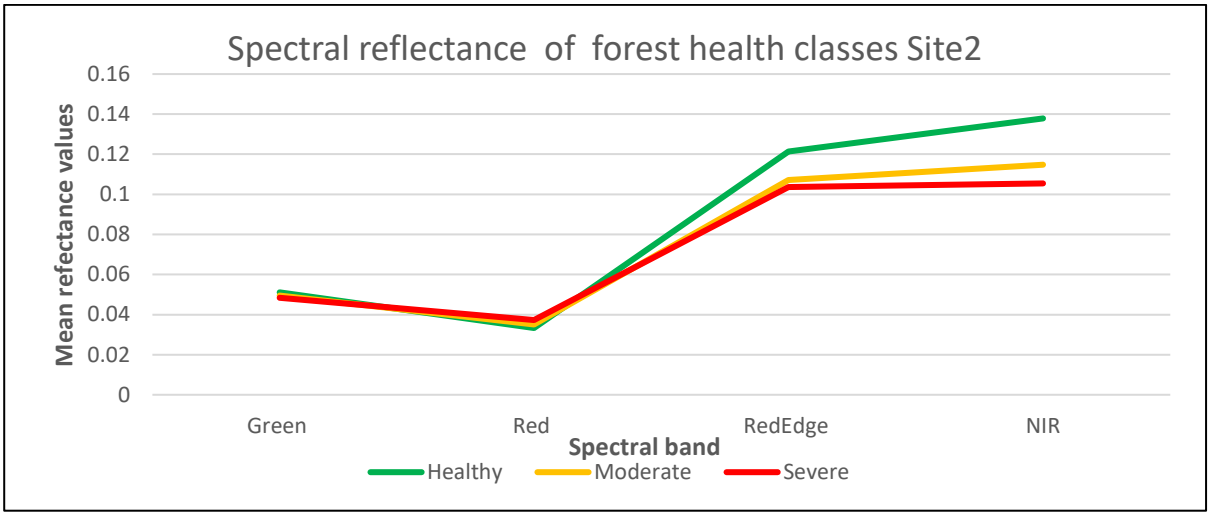

Figure 25: Spectral reflectance of forest health status site 2

4.5. Statistical Comparison of classes within the vegetation indices

Within the vegetation indices in both sites, the ANOVA results indicated that there is a statistical difference between the forest health classes at 95% confidence level. As for post hoc analysis, all the class pairs in all the vegetation indices showed that there was statistically significant difference between them except for severe and moderate class which showed that there was no statistical difference in NDRE index. The confidence level used was 95%. Table 8 and Table 9shows the ANOVA and post hoc calculated results from both sites.

Table 8: ANOVA test in sites 1 and site 2

Index	P-value site 1	P-value site Site 2
NDRE	4.41E-05	4.41E-05
NDVI	1.08E-05	1.08E-05
SAVI	4.96E-06	4.96E-06

Table 9:Post hoc analysis results

Index	health status pairswise	P-value site1	P values site 2
NDRE	Healthy-severe	0.00002	7.65E-06
	Healthy-moderate	0.04326	0.036
	severe -moderate	0.06604	0.072
NDVI	Healthy-severe	5.48E-06	4.44E-06
	Healthy-moderate	0.026	0.027
	severe -moderate	0.037	0.039
SAVI	Healthy-severe	2.47E-06	6.43E-06
	Healthy-moderate	0.0113	0.01
	severe -moderate	0.043	0.032

4.6. Separability analysis of classes within vegetation indices

In site 1 the NDVI separability between class healthy and moderate was 1.7, healthy and severe was 2.8 and moderate and severe 0.9. As for SAVI, the separability between healthy and moderate was 2.8 healthy and severe was 3.2 and moderate and severe 1.7. NDRE had a separability value for healthy and moderate as 1.21 healthy and severe was 1.4 and moderate and severe was 0.99. Generally, the highest separability between classes was observed in with SAVI while NDRE had the lowest separability between the classes as shown in Table 10.

Table 10: Separability values for the vegetation indices site 1

Vegetation index	Separability between classes (S)		
	S (Healthy-Moderate)	S(Healthy-Severe)	S(Moderate-Severe)
NDVI	1.733671	2.8154	1.645754
SAVI	2.797303	3.170581	1.676431
NDRE	1.215682	1.429972	0.989427

In site 2 the NDVI separability between class healthy and moderate was 1.4, healthy and severe was 1.8 and moderate and severe 0.8. As for SAVI, the separability between healthy and moderate was 1.6 healthy and severe was 2.5 and moderate and severe 1.7. NDRE had a separability value for healthy and moderate as 1.21 healthy and severe was 1.3 and moderate and severe was 0.73.Similary as observed in Table 11 SAVI had the highest separability between classes while NDRE had the lowest separability.

Table 11:Separability values for the vegetation indices site 2

Vegetation Index	Separability between classes (S)		
	S (Healthy-Moderate)	S(Healthy Severe)	S(Moderate-Severe)
NDVI	1.433344	1.832791	0.883748
SAVI	1.642345	2.457594	1.613642
NDRE	1.344841	1.303326	0.730203

4.7. Classification of the created segments

Figure26, Figure27, Figure28 and Figure 29 show the classification map results of site two based on NDVI, NDRE, SAVI and the combination of all the vegetation indices while Figure 30, Figure 31, Figure 32 and Figure33 shows the same classification results in site 2.From the classification results in both sites, it is evident that differences in the classification results exist both between vegetation indices as well as between classification algorithm used. For example, in some insatnces the use different classifiers on the same VI resulted in the same trees being classified differently. Similarly, in some instances, the same trees also have been assigned different class when a different vegetation index is used.

It can be noted from the results in both sites that the different vegetation indices generated more or less of one class of forest health than the other, for example, it can be noted in site 2 that more of the moderate class was generated with NDVI as compared to the NDRE. The different classification result acquired by different vegetation indices can be seen to have greatly influenced also the overall accuracy of the generated maps.

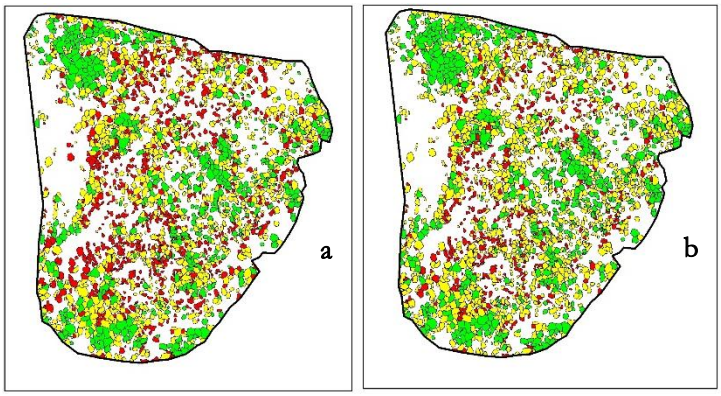

Figure26: site 1; (a) RF classification using NDVI (b) SVM classification using NDVI

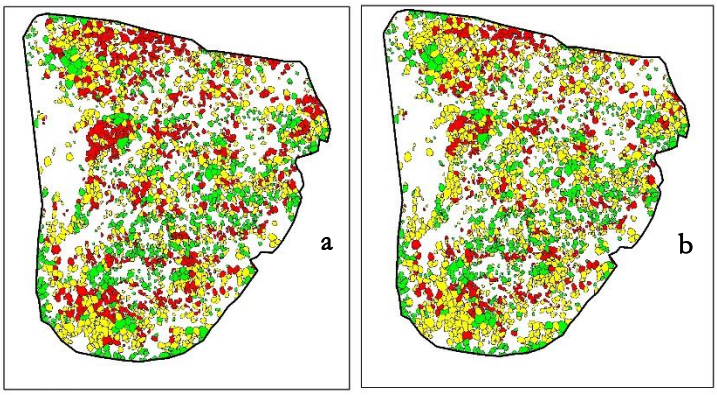

Figure27:site 1;(a) RF classification using NDRE (b) SVM classification using NDRE

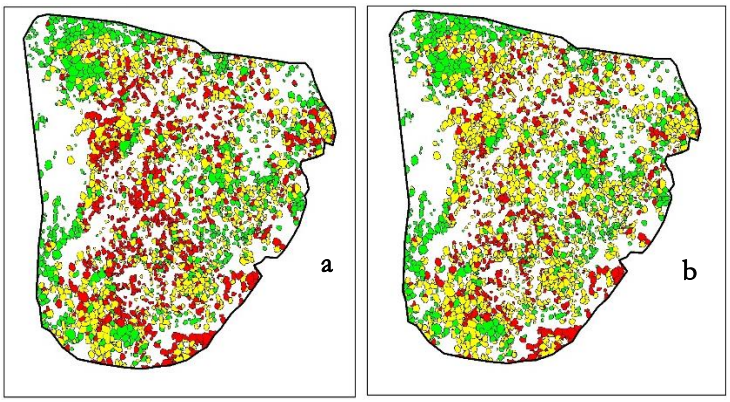

Figure28:site 1;(a) RF classification using SAVI (b) SVM classification using SAVI

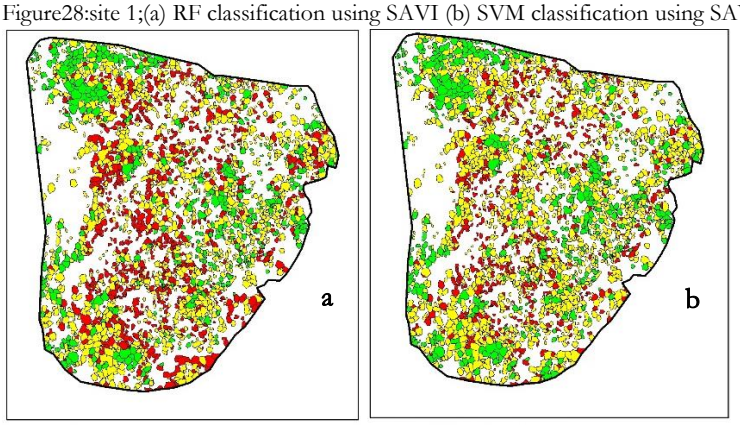

Figure 29: site 1;(a) RF classification using all the vegetation (b) SVM classification using all the vegetation indices combined.

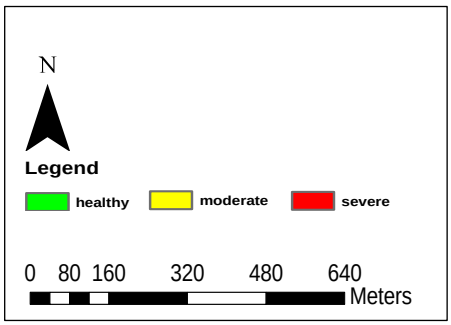

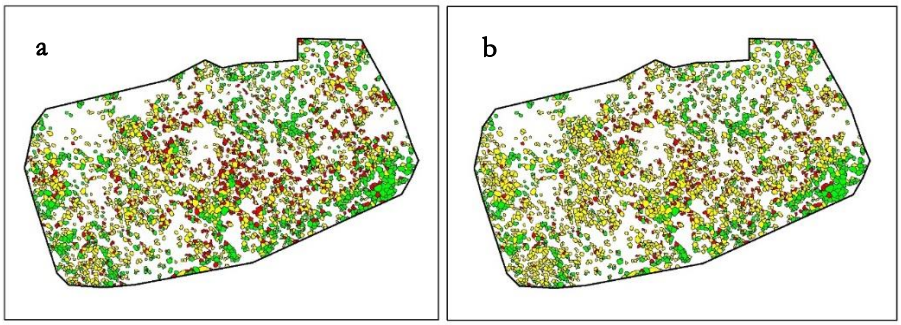

Figure 30: site 2; (a)Random forest classification using NDVI (b) SVM classification using NDVI

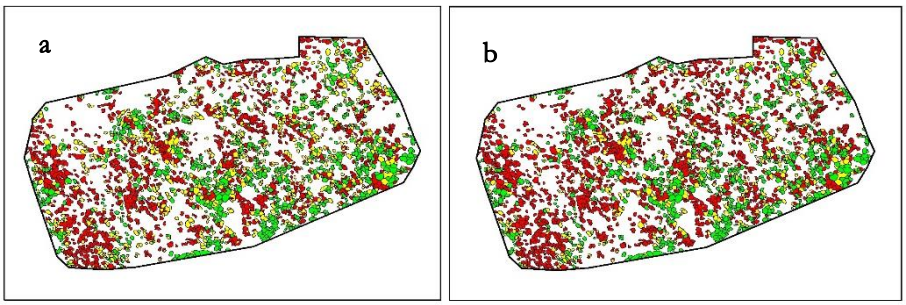

Figure 31:site 2; (a)Random forest classification using NDRE (b) SVM classification using NDRE

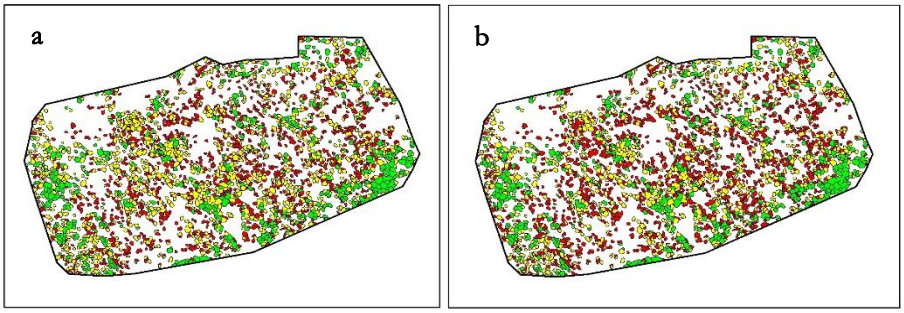

Figure 32:site 2; (a) RF classification using SAVI (b) SVM classification using SAVI

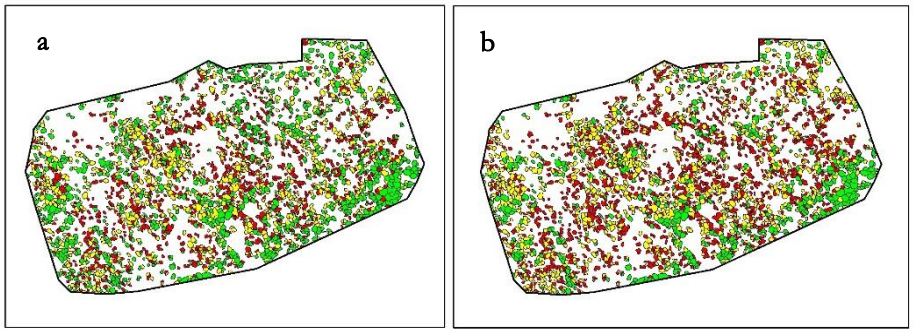

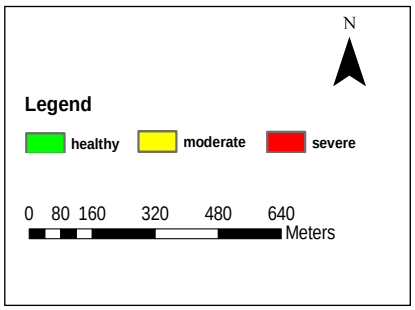

Figure33:site2;(a) RF classification using all the vegetation(b) SVM classification using all the vegetation indices combined.

4.8. Accuracy assessments

4.8.1. Accuracy assessment site 1

In site1 Random forest classifier had SAVI obtain an overall accuracy of 79%. SAVI can detect healthy, moderate and severe trees with 80%, 75%, and 82% accuracy respectively. For NDRE, the overall accuracy achieved is equal to 63% with a kappa statistic of 0.63. The capability of detection of healthy, moderate and severe trees, using NDRE, is 82 %, 53% and 100 respectively. The overall accuracy of NDVI is 76%. The moderate, healthy and severe can be distinguished in the field with the accuracy of 90 %, 64%, and 78%

respectively. All the vegetation indices combined can detect Healthy, moderate and severe trees with an accuracy of 90 %; 77% and 82% respectively. Tables 12, shows the summury of confusion matrix in all vegatattion indices using RF classifier.

Table 12: Results of error matrices site1using RF

Random forest Classifier	NDVI		NDRE		SAVI		Combined Vegetation Indices	
	User accuracy	Producer accuracy	Users accuracy	Producers accuracy	Users accuracy	Producers Accuracy	Users accuracy	Producers accuracy
Healthy	90%	90%	82%	90%	89%	80%	90%	90%
Moderate	64%	75%	53%	83%	69%	75%	77%	83%
Severe	78%	64%	100%	27%	73%	82%	82%	82%
Overall accuracy	78%		66%		79		85%	
Kappa	0.63		0.49		0.68		0.77	

When SVM classifier was used, the overall accuracy of the classification accounted for was 73% with a kappa statistic of 0.59 using NDVI. Furthermore. NDVI had user accuracy of 89%, 62% and 73% for class healthy moderate and severe respectively. The overall accuracy generated when SVM was used to classify NDRE was 64 % with a kappa statistic of 0.43, while the user accuracy obtained in the class healthy, moderate and severe were 90% 53% and 100% respectively. As for SAVI, the user accuracy obtained was 89% 63% and 88% for class healthy moderate and severe respectively, while the overall accuracy was 77% with a Kappa statistic of 0.63. Subsequently when all the vegetation indices were used for classification user's accuracy in healthy, moderate, and severe were 90, 71, and 89% respectively. Tables 13, shows the summury of confusion matrix in all vegatattion indices using SVM classifier in site 1.

Table 13: Results of error matrices site1 using SVM

SVM classifier	NDVI		NDRE		SAVI		Combine Vegetation Indices	
	User accuracy	Producer accuracy	Users accuracy	Producers accuracy	Users accuracy	Producers Accuracy	Users accuracy	Producers accuracy
Healthy	89%	80%	80%	80%	89%	80%	90%	90%
Moderate	62%	67%	50%	83%	63%	83%	71%	83%
Severe	73%	73%	100%	27%	88%	64%	89%	73%
Overall accuracy	73%		64%		77%		82%	
Kappa	0.59		0.43		0.63		0.73	

4.8.1. Accuracy assessment site 2

The overall accuracy of random forest classifier in Site 2 using SAVI achieved an overall accuracy of 72%. SAVI can detect healthy, moderate and severe trees with 75%, 60% and 79% of accuracy respectively. For NDRE, the overall accuracy achieved is equal to 61% with a kappa statistic of 0.41. Its capability of detecting of healthy, moderate and severe trees, using is 69%, 50%, and 58% respectively. The overall accuracy of NDVI is 61%. The moderate, healthy and severe trees can be distinguished in the field with the accuracy of 88% 50% and 100% respectively. All the vegetation indices combined can detect Healthy, moderate and severe trees with accuracy 91 %, 70, and 73% of accuracy respectively.

Table 14: Results of error matrices site2 using RF

Random forest Classifier	NDVI		NDRE		SAVI		Combine Vegetation Indices	
	User accuracy	Producer accuracy	User accuracy	Producers accuracy	Users accuracy	Producers Accuracy	Users accuracy	Producers accuracy
Healthy	88%	64%	69%	82%	75%	82%	91%	91%
Moderate	50%	92%	50%	17%	60%	50%	70%	58%
Severe	100%	46%	58%	85%	79%	85%	73%	85%
Overall accuracy	67%		61%		72%		78%	
Kappa	0.50		0.41%		0.58%		0.67	

When SVM classifier was also used, the overall accuracy of the classification accounted for 64% with a kappa statistic of 0.46 for NDVI. The user accuracy of 88%, 48% and 100% for class healthy moderate and severe respectively were further obtained with the use of NDVI. The overall accuracy generated when SVM was used to classify NDRE was 58 % with a kappa statistic of 0. 37 while the user accuracy obtained in the class healthy, moderate and severe were 69% 33% and 55% respectively. As for SAVI, the user accuracy obtained was 82% 63% and 65% for class healthy, moderate and severe respectively while the overall its accuracy was 70% with a Kappa statistic of 0.54. Also, when all the vegetation indices were used for classification a user's accuracy in healthy moderate, and severe were 90%, 70% and 69 % respectively. Tables 13, shows the summury of confusion matrix in all vegatattion indices using SVM classifier in site 2.

Table 15Results of error matrices site 2 using SVM

SVM classifier	NDVI		NDRE		SAVI		Combine Vegetation Indices	
	User accuracy	Producer accuracy	Users accuracy	Producers accuracy	Users accuracy	Producers Accuracy	Users accuracy	Producers accuracy
Healthy	88%	86%	69%	82%	82%	82%	90%	82%
Moderate	48%	92%	33%	8%	63%	42%	70%	58%
Severe	64%	46%	55%	85%	65%	85%	69%	85%
Overall accuracy	64%		58%		70%		75%	
Kappa	0.46		0.37		0.54		0.62	

4.9. Post classification analysis

The best method of classifying forest health classes from the study was found to be when using all the vegetation indices combined using random forest classifier. In site 1 the accuracy attained from random forest classifier with the use of all vegetation indices combine was found to be 84% while in site 2 the accuracy achieved was 78 %. The results generally show the severe, moderate and healthy class to be distributed throughout the study area in both sites. However, the results of site 2 could have been affected by sun illumination difference because the UAV flights were conducted in the forenoon. The maps that attained these accuracies were further converted into polygons in Arc GIS and area covered by each class was calculated in hectares. In site one, area covered by moderate class was approximately 9.386 hectares healthy class was 4.485 and lastly, the severe class was 5.275. Similarly, in site two the area covered by

moderate class is 4.835 hectares, healthy is 5.137 and severe is 3.479. Figure 34 and Figure 36 show the finals maps generated while Figure 35 and Figure 37 show the generated bar graphs showing the areas covered by each class in both sites.

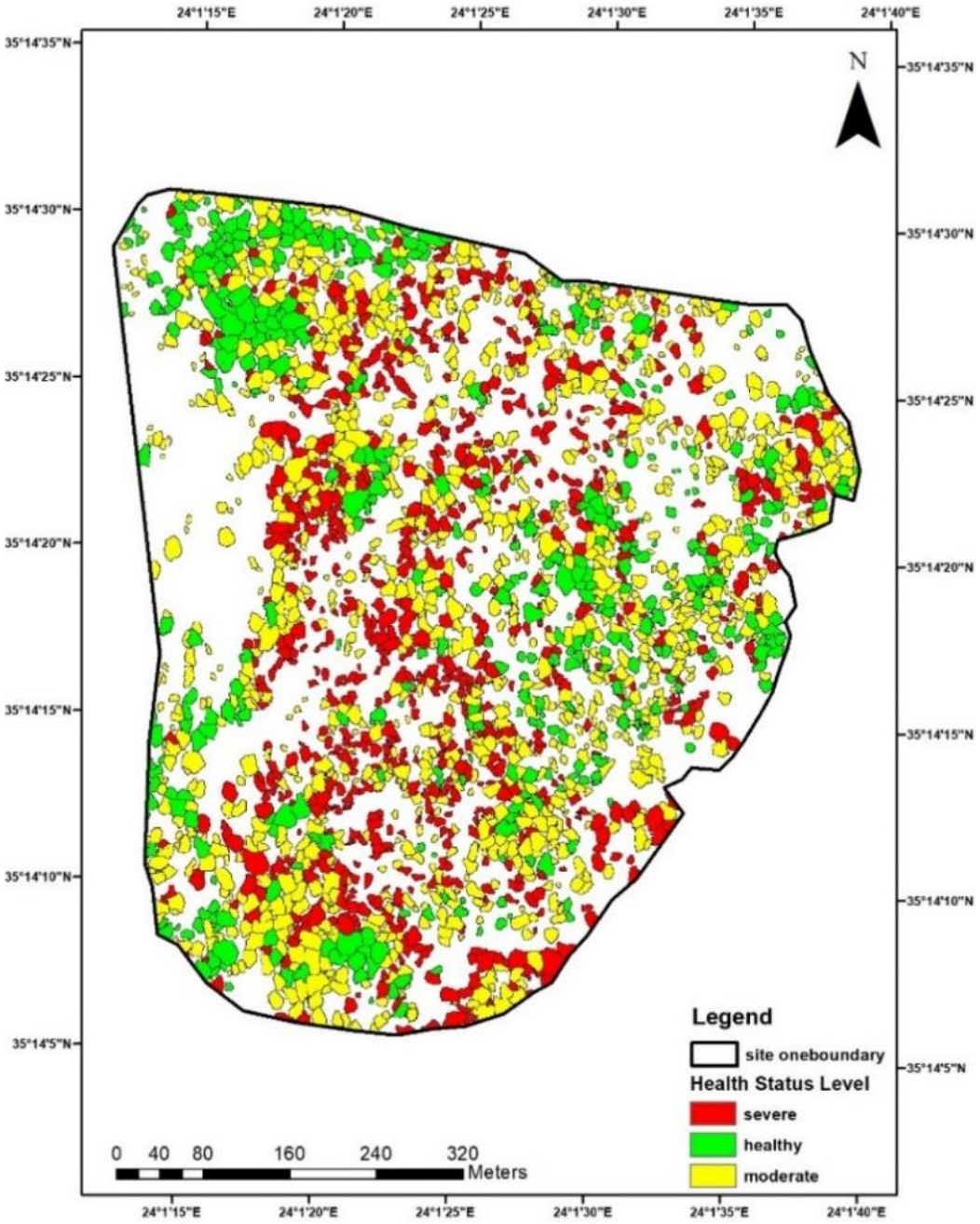

Figure 34: Final forest health map site 1

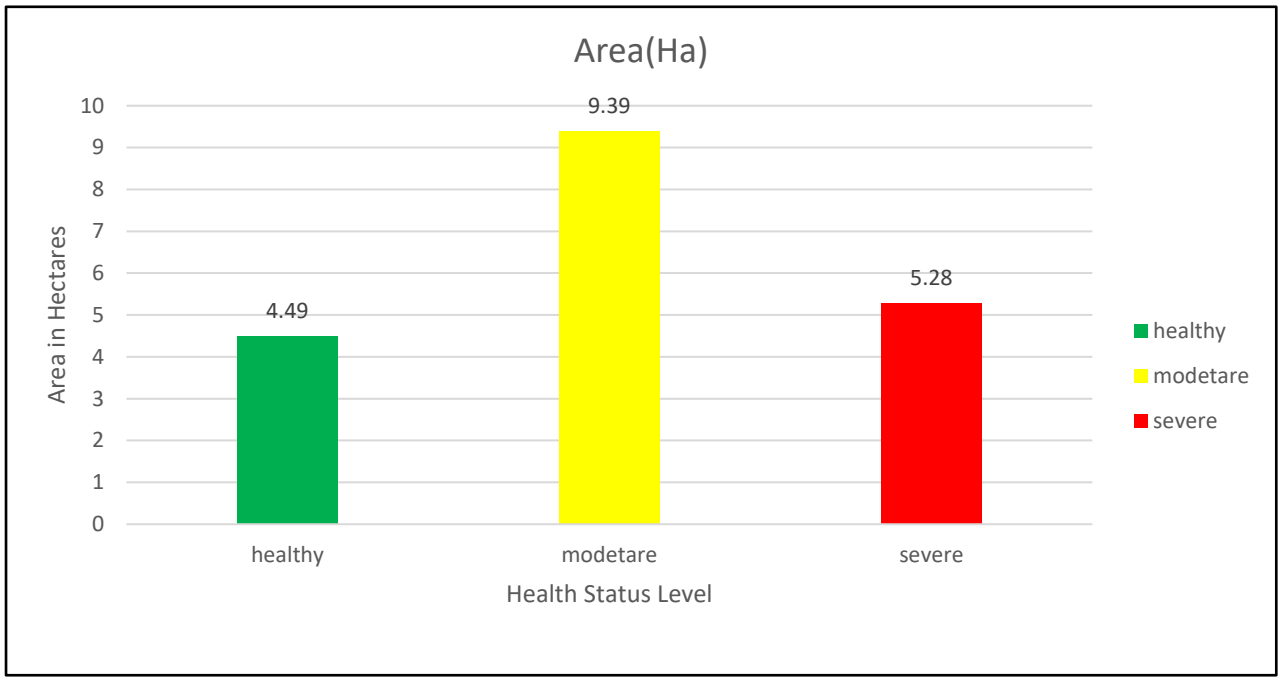

Figure 35: Area in Hectares covered by each class in site 1

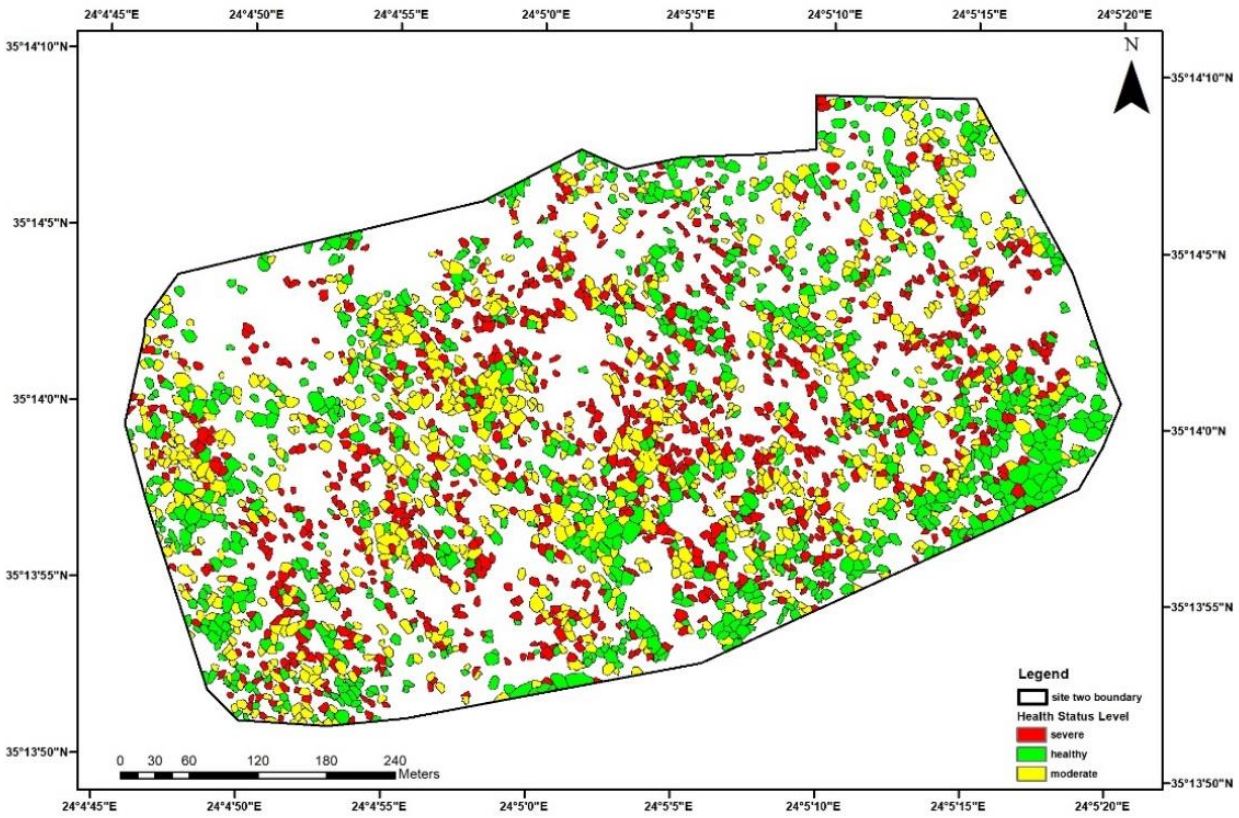

Figure 36: Final forest health Map site 2

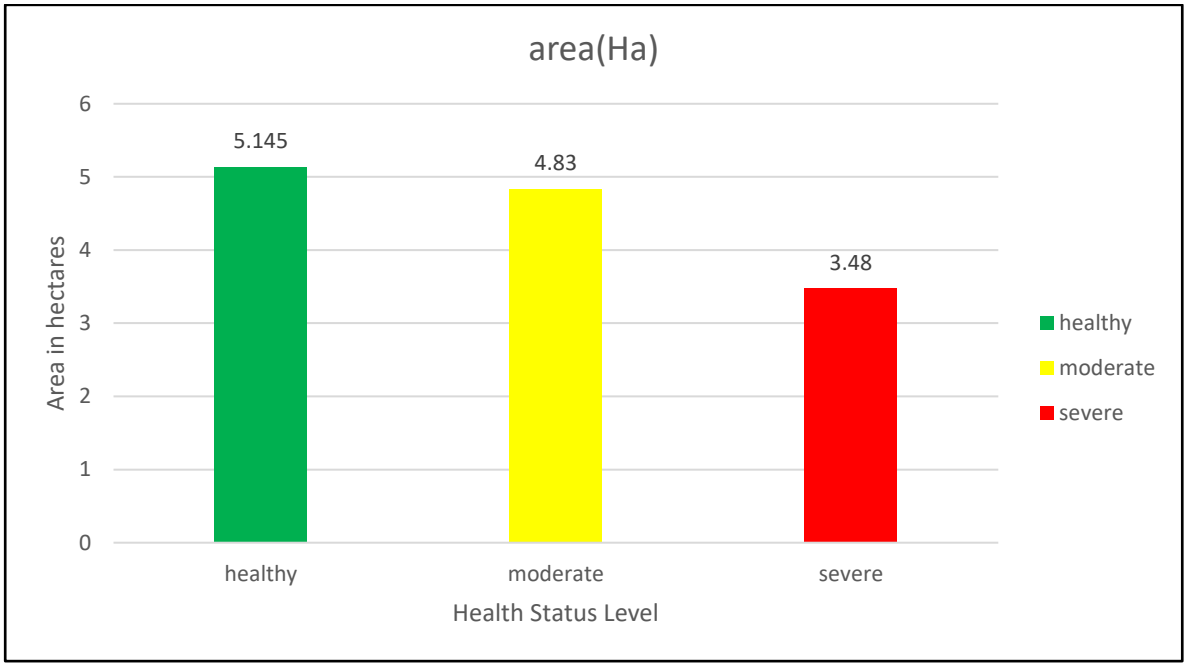

Figure 37: Area in Hectares covered by each class in site 2

5. DISCUSSION

5.1. Image Segmentation and Accuracy Assesment

The use of multi-resolution segmentation was seen as the best algorithm for segmentation because it is able to take into account forests that are highly heterogeneous. This is not as compared to the other algorithms which always considers the shape of the tree to be cone-shaped and the brightest part of the tree to be representing the crown. The consideration of the brightest part of the tree to be a crown and assumption that the tree crown is conical in shape is a perfect example of planted and managed trees or forest (Culvenor 2002; Gonzalez et al. 2010). In this case, the forest in the study was somehow complex as it contained naturally growing pine and cypress trees that were not managed, the trees were of different ages with different crown shapes, the branches of the trees were uniquely positioned and different illumination from the trees. Therefore, other segmentation algorithms could not be able to factor in this complexity as compared to multiresolution segmentation which forms crown segments while taking into account spectrally and spatially similar pixel (Wang et al. 2010).

The segmentation accuracies in this study were achieved on a one to one relationship matching between the automatically generated segments from ecognition and the manually delineated tree crowns (references). The segmentation accuracy for Site 1 and Site 2 were 81 %and 76% respectively. These segmentation accuracies are considered to be high. The most probable reason for high segmentation accuracy could be that the segmentation was carried out in an open forest with single dispersed trees with high contrast bare ground in between the trees. Segmentation in such ecosystem would be rather successful compared to a dense forest with overlapping tree canopies. Secondly, the high accuracy could also have been attained because manual delineation was only done on the tree samples that were recognized in the field rather than randomly selecting the trees from both sites.

The obtained segmentation accuracy results were common to those achieved by Wang et al. (2004) who achieved an accuracy of 75.6% while segmenting tree crowns from non-tree crowns. Mohan et al. (2017) achieved an accuracy f-score of 86% while detecting individual trees in an Open Canopy Mixed Conifer Forest. Huang et al. (2018) obtained an accuracy with f-score 98.2% and 93.1% while using watershed segmentation to delaminate individual tree crowns of *Osmanthus* and *Podocarpus* trees in an open forest. Ke et al. (2008) obtained an accuracy of 61.3% while delineating tree crowns in mixed broad leaves and needles trees using region growing segmentation algorithm.

Site two had lower segmentation accuracy as compared to the site 1 because the second site had uncertainties related to shadows cast by the trees as images were aquired at forenoon.Taller trees overshadowed neighbouring shorter trees introducing low reflectance and reduced segmentation accuracy; Also, some of the shadows were segmented as trees affecting both segmentation and classification further on.

One major challenge faced in both sites was the natural forest had trees that were unmanaged; hence the some of the branches in the trees were protruding and in some case were confused as crowns. This slightly affected the segmentation and further the classification accuracy.

5.2. Separability of classes between vegetation indices

High separability results between classes were obtained with SAVI followed by NDVI while NDRE had the lowest separability values between classes. This shows that, with SAVI, the forest health classes can be differentiated better as compared to the NDVI and NDRE. The reason for high separability of classes within SAVI could be because of its countermeasure for the effect of soil brightness which normally affects the calculation of vegetation indices in areas where the vegetation is low. This could mean that the values that are generated from SAVI representing different class could have been more different from each other as compared to the other vegetation indices which do not offer this counter-effect measures and are easily influenced by soil brightness. It was noted that separability between class healthy and severe generally was higher as compared to moderate and severe in all the three vegetation indices. The separability between class severe and moderate was the lowest across all the vegetation indices indicating the difficulty in their separation within the vegetation indices. The reason for this low separability value could be because the vegetation indices values that separates them might have been close to each other. This could be attributed to the lack of clearly visible difference in the reflectance values between the moderate healthy trees and the severely healthy trees .

Comparable separability tests between classes within vegetation indices have been performed by Tuominen et al. (2009).Their research was looking how easy was it for the vegetation indices calculated from Hy map airborne hyperspectral scanner to separate between healthy and defoliated trees. Their result showed that NDVI had the highest separability value among the 16 vegetation indices. Adamczyk & Osberger (2015) also Performed a separability analysis for ten vegetation indices calculated from Rapid Eye, whereby, among the ten VIs they found two most suitable vegetation indices (NDVI and NDRE) for threshold OBIA classification. Their separability outcomes would be different from the once achieved from this study because of the use of a different remotesensing platform with different characteristic as from the one used in this study.

5.3. Forest health classification accuracy

The difference in classification performance of indices is seen by the outcome in maps, whereby for instance the same trees are classified differently across different vegetation indices. This can be due to the different levels of separability and sensitivity of the different vegetation indices as seen in the separability
Table 10 and Table 11. The overall classification accuracy gives poor results for NDRE vegetation indies, moderate classification results using NDVI, better results using SAVI vegetation indices and much better results when all the vegetation indices are combined. This is the true case across all the classifier used. The reason for higher classification accuracy when all the vegetation indices were combined could be because different vegetation indices are able to highlight special characteristic of vegetation that the other one cannot address so when they are combined together, they are able to complement each other, resulting to higher accuracies. Dash et al. (2017) also found out that using all the four vegetation indices (NDVI, green NDVI, NDRE and the nonlinear index) in random forest classification models produced higher kappa statistics than when individual vegetation indices are used.

From all the generated confusion matrix in this research, it can be noted that the user accuracy generated by moderate class are generally low compared to other classes. This shows that there is a higher chance that the class moderate on the map does not really represent the moderate healthy trees on the ground. However, across all the vegetation indices in both study areas it was noted that the user accuracy of the class healthy was very high this indicates that there is a likelihood that the class healthy on the map truly represents the healthy trees on the ground. As for the class severe, the user accuracy fluctuated between moderate user

accuracy and higher user accuracy with some vegetation indices recording high user accuracy and others recording moderate user accuracy across the two sites. Generally, the user accuracies produced depended highly on the type of vegetation indices that were used to classify the status of forest health. The reason for higher user accuracy in the healthy class was that fewer or none of the healthy class that were misclassified or wrongly classified into other classes as clearly shown in the confusion matrices in the appendices. The low user accuracies obtained from the class moderate and the fluctuating user accuracies obtained from the class severe can be due to the fact that differentiating between the moderate and the severe with the classifier was difficult within the vegetation indices leading to the misclassification between the two classes. Furthermore, the samples that were collected were not enough to be able to provide much variations between the moderately healthy and severely healthy trees, and this can be seen in the confusion brought in during the classification where some of the moderate class were being classified as severe and some of the severe class being classified as moderate. The issues of misclassification are common during classification and have been experienced with other studies. For example, while classifying the hyperspectral imagery into five classes (Bare soil, Healthy Broadleaves, Healthy Coniferous ,Dead trees ,vegetated soil) to map bark beetle-induced tree mortality, Fassnacht et al. (2014) found out that most of the confusion of misclassification occurred between dead trees and sparsely populated vegetated soil further affecting their user accuracies . Their Studies confirms that the issues of misclassification or confusion can happen.

The overall forest health classification accuracies achieved in this study can be compared to Dash et al. (2017) where they compared different vegetation indices, i.e. NDVI, green NDVI, NDRE and the nonlinear index (NLI) in simulated dense forest disease attacks. They found out that different vegetation indices performed differently when monitoring and assessing the levels of forest health. Their results showed that individually the best vegetation index in detecting physiological stress was the NDVI with a Kappa statistic of 0.57, the green NDVI came in second with a kappa statistic of 0.484 while the least performance was NLI with a kappa statistic of 0.39. From their findings, it was noted that individual vegetation indices performed poorly as compared to when all of them are combined. Their results achieved very kappa statistic of 0.64 when all the four vegetation indices were combined as compared to the individual vegetation indices. This is similar to the finding of this study where the use of all the vegetation indices combined produced the highest kappa statistics across both sites. Näsi et al. (2015) used hyperspectral images acquired from UAV images to classify Norway spruce forest that had been attacked by European spruce bark beetle into three classes, i.e., infested healthy and dead. The overall accuracy achieved by their classification while using k-nearest neighbour non-parametric classifier was 76% with kappa statistics of 0.6. Lehmann et al. (2015) obtained a kappa statistic accuracy of 0.81 and 0.76 at two study sites while classifying five levels of an infested oak forest using NDVI. Näsi et al. (2018) Classified the beetle damage in urban forests at individual tree level using a novel hyperspectral camera from UAV and was able to obtain an accuracy of 81% and kappa statistics of 0.70 also while using k-nearest neighbour classifier.

In this study, three classes (healthy, moderate, severe) were used to categorize the forest health status with moderate being the intermediate class. Working with the intermediate class could also be the cause affecting the overall classification accuracy. Some studies have shown that working with intermediate classes lowered the overall percentage accuracy or kappa values. For example, Näsi et al. (2015) found out that when classifying his forest health status using three classes (healthy, infested and dead) his kappa statistic was 0.6 as opposed to when he used healthy and dead which achieved a kappa of 0.8. His finding showed that removing the intermediate class 'infested' increased the kappa statistics value. Dash et al. (2017) also found high and perfect classification results when using severe discoloration and healthy as opposed to intermediate classes such as moderate as he had earlier tested. These two examples show that using extremes classes of physiological stress can increase accuracy as opposed to the use of intermediate classes.

Looking at the vegetation indices individually the highest overall accuracy was achieved when using SAVI was used to classify forest health classes while NDRE had the poorest overall classification compared to the rest. This was unexpected as the NDRE is known to apply all the values along the red edge region making it sensitive to slight changes that occur within vegetation. High accuracy using red edge have been reported with different studies which are in contrary to what this study has found. For example, Adamczyk & Osberger (2015) found out that red edge was more accurate in detecting stress early enough on conifer trees as compared to NDVI although the forest under study was dense as compared to the open forest in this present study . Other studies have shown the NDRE to perform moderately.For example Dash et al. (2017) found out that the NDREcame in second when after NDVI in terms of performance when they were used to assess the different level of forest health stress in a simulated forest diseases attack. A possible reason for low accuracy with the use of NDRE in this study might be that assessment of tree health in the field was based only in the defoliation status, whereas, there are many indicators and environmental factors that could have been more useful training the datasets and were not collected at the time. These datasets could not have been collected within the timeframe of this study. Furthermore, data collected was only restricted to human vision (categorizing defoliation status). Collecting data on defoliation when the tree is less defoliated it does not mean it is unhealthy.

The tree crowns in site 2 had diameter ranges of 2-5 metres. This significantly affected the classification and accuracy assessment due to the fact that the handheld GNSS used to collect the tree sample had an accuracy of 3-5 meters. The location of most of the trees that had a diameter of less than 3 meters was not adequately identified leading to low classification accuracy and more misclassifications as compared to site 1. The effect of light (over exposed or under exposed had) could have had a negative implication on overall classification accuracy especially in site 2 where the flight was conducted early morning before noon when the lighting conditions were not the best. In site 2 you find that due to the different exposure of sunlight to the trees the reflectance values of the trees were affected, with trees exposed to more sunlight reflecting more. These means that a healthy tree that is not exposed to sunlight will reflect less NIR as compared to the healthy tree exposed to sunlight and the same compared to the moderate class that is exposed to sunlight. These would further affect the classification leading misclassification and confusing within the vegetation indices. The illumination issues, therefore, could not be completely be reduced by the vegetation indices. This can, therefore, be reduced by conducting UAV flights at noon time or during closed cloud cover.

5.4. Comparison of the two Classifiers

Random forest classifier achieved slightly higher accuracy than SVM. There is no big difference between the classification performed by RF or SVM. In the generated forest health maps, it can also be seen that the classifiers performed slightly differently when used to classify the same objects represented through different vegetation indices. For example, the same tree is assigned a different class when the two classifiers are used in the same vegetation index. The difference in results between random forest and SVM can be due to the difference in the algorithm design that are used by the classifiers to perform the classification. These algorithms would determine how best to classify different classes that are even very difficult to differentiate from each other. For example, SVM uses hyperplanes to separate classes while random forest uses a group of decision trees for classification explaining the reason for the slightly different in classification outcome and accuracy assessments results. Similar comparisons have been made between non-parametric classifiers in the field of forest health assessment, for example, Abdel-Rahman et al. (2014) compared how random forest (RF) and support vector machines (SVM) classifiers in distinguishing amongst healthy, sirex grey-attacked and lightning-damaged pine trees using AISA Eagle hyperspectral data. Their results showed that

random forest achieved slightly higher accuracy of 74.5% than the SVM which attained an accuracy of 73. Their study concluded that the two non-parametric classifiers performed comparatively the same in classification of the eight classes, although the RF achieved higher overall accuracy. Their finding is similar to this present study that showed the overall accuracy attained by RF slightly edging out SVM with very small margins in the overall accuracy.

5.5. The use of the Parrot Sequoia multispectral camera

The achieved results from the Parrot Sequoia camera was promising, particularly in site two where the classification accuracy results were very suitable when RF classifier was used. Therefore, using a UAS multispectral acquired imagery can be a helpful tool in forest health management both for forest manager and private forest owners. As presented in this study, the identification of the three different forest classes is possible and permits for a first evaluation of the dimension of damage in the forest stand. The use of multispectral band enables the detection and assessment of trees. However, this is not a diagnosing tool that should be providing information for the reason of stress in trees. In the case of this study, multifactorial processes are related to the damage and decline of the forest. Besides the biotic factors such as pest and several abiotic factors such as drought are also implicated in the damages of trees. In this study drought combine with pest infestation was the main reason for defoliation and discoloration of altering the canopy reflection signatures of the trees understudy. Thus, identifying the reason for stress in trees using UAV is limited because of the reason that several factors as mentioned earlier would result in similar features. Although this drawback exits on the use of UAS, it can support ground surveys that are visually conducted as in this study. This is because field surveys at times can be expensive and time-consuming.

5.6. Limitation in the research

The limitation in this study is limited accessibility to study area (as a result of fluctuating terrain) that can lead in the probable absence of ground-based GCPs which are very crucial in calculating the correct exterior orientation of the image. Although the parrot sequoia camera had its GPS and IMU onboard, the accuracy from its GPS has a positional accuracy of 3-5 meters which is low for direct processing of the image exterior orientation. Research on how to put onboard enhanced DGPS onboard UAV are currently underway which would allow for accurate instant georeferencing hence improving the exterior orientation of the images acquired under such circumstances.

6. CONCLUSION AND RECOMMENDATION

6.1. Conclusion

The result obtained from this work showed that it was feasible to classify and identify individual trees affected at different level by pest infestation. This is as opposed to the traditional remotesensing methods of medium and high-resolution satellite. The Sequoia collected images were used to calculate vegetation indices which were later used classify the levels of forest health. The proposed method in this research included the use of Sequoia camera to acquire an image, mosaicking of the UAS images, preprocessing of the mosaiced images, calculation of vegetation indices, multiresolution segmentation, segmentation accuracy, classification and accuracy assessment and calculation of areas covered by different classes of the forest health status. This research had 3 objectives and six questions the specific conclusions are presented below:

Question1: What accuracy is obtained when NDVI is used to classify forest health?

The overall classification accuracy attained when NDVI was used to classify forest health classes the were moderate results across the two classifiers in both sites. In site 1, the classification by NDVI attained an accuracy of 78% and 75% when using RF and SVM classifier respectively. In site two RF and SVM achieved an accuracy of 67% and 64%b respectively.

Question2: What accuracy is obtained when SAVI is used to classify forest health?

SAVI was able to achieve much better results than NDVI with an accuracy of 79 and 77% within RF and SVM in site 1. Whereas in site 2 RF and SVM attained an accuracy of 72% and 70% respectively.

Question3: What accuracy is obtained when NDRE is used to classify forest health?

NDRE obtained the lowest overall classification accuracy of the forest health class with site 1 achieving accuracies of 66% and 64% in RF and SVM respectively. While sites 2 obtained an overall accuracy of 61 % and 58% in RF and SVM respectively.

Question4: What accuracy is obtained when all the vegetation indices are combined to classify forest health classes?

Combination of the of all vegetation indices showed an increase in the overall classification of forest health. The use of the combination generated the highest accuracy in this study with site 1 have an overall accuracy of 84% and 82% within RF and SVM respectively. In site 2 still, the overall accuracy was highest with an accuracy of 78 and 75 when using RF and SVM respectively.

Question5: What is the performance of the two different classifier different classifiers?

This research concluded that the two non-parametric classifiers performed comparatively the same in classifying forest health classes although the RF achieved a slightly higher overall accuracy over SVM.

Question6: What is the area covered by different forest health classes?

In site one area covered by moderate class was approximately 9.39 hectares healthy class was 4.49 and lastly, the severe class was 5.28. Similarly, in site two the area covered by moderate class is 4.84 hectares, healthy is 5.137 and severe is 3.48.

6.2. Recommendation

The results from the research used only few training samples for the analysis, i.e., 109 in site and 125 samples in site 1 this can be linked to not obtaining more accuracy assessment and kappa statistics. Therefore, there is a need to increase the number of samples collected in the subsequent works. It is crucial to include other characteristics for object-based classification, for example, texture, shape etc. Future research in this area should concentrate on looking at different time intervals of the collected images in order to be able to monitor the time series of the images and asses changes that occur on the individual trees. Future additional characteristics and indicators and environmental factors should also be included or accommodated during classification. Modeling factors affecting the Mediterranean forest should be the subject of future studies. Future research should use RTK GNNS during data collection. This would increase the accuracy of the samples collected and possibly result in higher classification accuracy.

LIST OF REFERENCES

Abdel-Rahman, E. M., Mutanga, O., Adam, E., & Ismail, R. (2014). 'Detecting Sirex noctilio grey-attacked and lightning-struck pine trees using airborne hyperspectral data, random forest and support vector machines classifiers', *ISPRS Journal of Photogrammetry and Remote Sensing*. DOI: 10.1016/j.isprsjprs.2013.11.013

Adamczyk, J., & Osberger, A. (2015). 'Red-edge vegetation indices for detecting and assessing disturbances in Norway spruce dominated mountain forests', *International Journal of Applied Earth Observation and Geoinformation*, 37: 90–9. Elsevier B.V. DOI: 10.1016/j.jag.2014.10.013

Al-Kindi, K. M., Kwan, P., R. Andrew, N., & Welch, M. (2017). 'Remote sensing and spatial statistical techniques for modelling *Ommatissus lybicus* (Hemiptera: Tropiduchidae) habitat and population densities', *PeerJ*. DOI: 10.7717/peerj.3752

Ali, S., & Gueaieb, W. (2010). 'Intelligent Flight Control of an Autonomous Quadrotor', *Motion Control*, 1. DOI: 10.5772/6968

Baatz, M., Schäpe, a, & Schäpe, A. (2000). 'Multiresolution Segmentation - an optimization approach for high quality multi-scale image segmentation'. *XII Angewandte Geographische informationsverarbeitung* . DOI: Export Date 6 May 2013

Baboo, S., & Devi, R. (2010). 'An Analysis of Different Resampling Methods in Coimbatore, District', *Global Journal of Computer Science and Technology*, 10/15: 61–6.

Bannari, A., Morin, D., Bonn, F., & Huete, A. R. (1995). 'A review of vegetation indices', *Remote Sensing Reviews*, 13/1–2: 95–120. Taylor & Francis. DOI: 10.1080/02757259509532298

Barton, C. V. M., & North, P. R. J. (2001). 'Remote sensing of canopy light use efficiency using the photochemical reflectance index model and sensitivity analysis', *Remote Sensing of Environment*. DOI: 10.1016/S0034-4257(01)00224-3

Blaschke, T. (2010). 'Object based image analysis for remote sensing'. *ISPRS Journal of Photogrammetry and Remote Sensing*. DOI: 10.1016/j.isprsjprs.2009.06.004

Calderón, R., Navas-Cortés, J. A., & Zarco-Tejada, P. J. (2015). 'Early detection and quantification of verticillium wilt in olive using hyperspectral and thermal imagery over large areas', *Remote Sensing*. DOI: 10.3390/rs70505584

Castello, J. D., & Teale, S. A. (2011). *Forest health: An integrated perspective*. *Forest Health: An Integrated Perspective*. DOI: 10.1017/CBO9780511974977

Chao, S. (2012). 'Forest peoples: numbers across the world', *Forest peoples: numbers across the world*, 24 pp. DOI: 10.1007/s00441-005-1116-6

Clinton, N., Holt, A., Scarborough, J., Yan, L., & Gong, P. (2010). 'Accuracy Assessment Measures for Object-based Image Segmentation Goodness', *Photogrammetric Engineering & Remote Sensing*. DOI: 10.14358/PERS.76.3.289

Congalton, R. G. (1991). 'A review of assessing the accuracy of classifications of remotely sensed data', *Remote Sensing of Environment*. DOI: 10.1016/0034-4257(91)90048-B

Coops, N. C., Johnson, M., Wulder, M. A., & White, J. C. (2006). 'Assessment of QuickBird high spatial resolution imagery to detect red attack damage due to mountain pine beetle infestation', *Remote Sensing of Environment*. DOI: 10.1016/j.rse.2006.03.012

Coops, N. C., Stanford, M., Old, K., Dudzinski, M., Culvenor, D. S., & Stone, C. (2003). 'Assessment of Dothistroma needle blight of Pinus radiata using airborne hyperspectral imagery', *Phytopathology*. DOI: 10.1094/PHYTO.2003.93.12.1524

Culvenor, D. S. (2002). 'TIDA: An algorithm for the delineation of tree crowns in high spatial resolution remotely sensed imagery', *Computers and Geosciences*. DOI: 10.1016/S0098-3004(00)00110-2

Dale, V. H. (2001). 'Climate Change and Forest Disturbances: Climate change can affect forests by altering the frequency, intensity, duration, and timing of fire, drought, introduced species, insect and pathogen outbreaks, hurricanes, windstorms, ice storms, or landslides', *BioScience*, 51/7: 555–6. DOI: 10.1641/0006-3568(2001)051

Damiand, G., & Resch, P. (2003). 'Split-and-merge algorithms defined on topological maps for 3D image segmentation', *Graphical Models*. DOI: 10.1016/S1524-0703(03)00009-2

Dash, J. P., Watt, M. S., Pearse, G. D., Heaphy, M., & Dungey, H. S. (2017a). 'Assessing very high resolution UAV imagery for monitoring forest health during a simulated disease outbreak', *ISPRS Journal of Photogrammetry and Remote Sensing*, 131: 1–14. Scion (New Zealand Forest Research Institute). DOI: 10.1016/j.isprsjprs.2017.07.007

——. (2017b). 'Assessing very high resolution UAV imagery for monitoring forest health during a simulated disease outbreak', *ISPRS Journal of Photogrammetry and Remote Sensing*, 131: 1–14. DOI: 10.1016/j.isprsjprs.2017.07.007
DeHayes, D. H., Schaberg, P. G., Hawley, G. J., & Strimbeck, G. R. (1999). 'Acid Rain Impacts on Calcium Nutrition and Forest Health', *BioScience*, 49/10: 789–800. DOI: 10.2307/1313570
Deng, L., Mao, Z., Li, X., Hu, Z., Duan, F., & Yan, Y. (2018). 'UAV-based multispectral remote sensing for precision agriculture: A comparison between different cameras', *ISPRS Journal of Photogrammetry and Remote Sensing*. DOI: 10.1016/j.isprsjprs.2018.09.008
Drăguţ, L., Tiede, D., & Levick, S. R. (2010). 'ESP: A tool to estimate scale parameter for multiresolution image segmentation of remotely sensed data', *International Journal of Geographical Information Science*. DOI: 10.1080/13658810903174803
Eitel, J. U. H., Vierling, L. A., Litvak, M. E., Long, D. S., Schulthess, U., Ager, A. A., Krofcheck, D. J., et al. (2011). 'Broadband, red-edge information from satellites improves early stress detection in a New Mexico conifer woodland', *Remote Sensing of Environment*, 115/12: 3640–6. DOI: 10.1016/j.rse.2011.09.002
Ellison, D., Morris, C. E., Locatelli, B., Sheil, D., Cohen, J., Murdiyarso, D., Gutierrez, V., et al. (2017). 'Trees, forests and water: Cool insights for a hot world', *Global Environmental Change*, 43: 51–61. Elsevier Ltd. DOI: 10.1016/j.gloenvcha.2017.01.002
Fassnacht, F. E., Latifi, H., Ghosh, A., Joshi, P. K., & Koch, B. (2014). 'Assessing the potential of hyperspectral imagery to map bark beetle-induced tree mortality', *Remote Sensing of Environment*. DOI: 10.1016/j.rse.2013.09.014
Fernández-Calzado, R., Ghosn, D., Gottfried, M., Kazakis, G., Molero Mesa, J., Pauli, H., & Merzouki, A. (2013). 'Patterns of endemism along an elevation gradient in Sierra Nevada (Spain) and Lefka Ori (Crete, Greece)', *Pirineos*, 168/0: 7–24. DOI: 10.3989/Pirineos.2013.168001
Finley, K., & Chhin, S. (2016). 'Forest Health Management and Detection of Invasive Forest Insects', *Resources*, 5/2: 18. DOI: 10.3390/resources5020018
Fischer, R., Mues, V., Ulrich, E., Becher, G., & Lorenz, M. (2007). 'Monitoring of atmospheric deposition in European forests and an overview on its implication on forest condition', *Applied Geochemistry*, 22/6: 1129–39. DOI: 10.1016/j.apgeochem.2007.03.004
Food and Agriculture Organization of the United Nations. (2009). 'Global review of forest pests and diseases', *FAO Forestry Paper 156*, 2: 222.
Franklin, S. E., Wulder, M. A., Skakun, R. S., & Carroll, A. L. (2003). 'Mountain Pine Beetle Red-Attack Forest Damage Classification Using Stratified Landsat TM Data in British Columbia, Canada', *Photogrammetric Engineering & Remote Sensing*. DOI: 10.14358/PERS.69.3.283
Gandhi, K. J. K., Gilmore, D. W., Katovich, S. A., Mattson, W. J., Spence, J. R., & Seybold, S. J. (2007). 'Physical effects of weather events on the abundance and diversity of insects in North American forests', *Environmental Reviews*, 15/NA: 113–52. Canadian Science Publishing. DOI: 10.1139/A07-003
Gonzalez, P., Asner, G. P., Battles, J. J., Lefsky, M. A., Waring, K. M., & Palace, M. (2010). 'Forest carbon densities and uncertainties from Lidar, QuickBird, and field measurements in California', *Remote Sensing of Environment*. DOI: 10.1016/j.rse.2010.02.011
Green, W., & Oh, P. Y. (2007). *Advances in Unmanned Aerial Vehicles. Advances in unmanned aerial vehicles: state of the art and the road to autonomy*, Vol. 33. DOI: 10.1007/978-1-4020-6114-1
Hart, S. J., & Veblen, T. T. (2015). 'Detection of spruce beetle-induced tree mortality using high- and medium-resolution remotely sensed imagery', *Remote Sensing of Environment*, 168: 134–45. Elsevier Inc. DOI: 10.1016/j.rse.2015.06.015
Havašová, M., Bucha, T., Ferenčík, J., & Jakuš, R. (2015). 'Applicability of a vegetation indices-based method to map bark beetle outbreaks in the High Tatra Mountains', *Annals of Forest Research*, 58/2: 295–310. DOI: 10.15287/afr.2015.388
Hicke, J. A., & Logan, J. (2009). 'Mapping whitebark pine mortality caused by a mountain pine beetle outbreak with high spatial resolution satellite imagery', *International Journal of Remote Sensing*. DOI: 10.1080/01431160802566439
Hódar, J. A., Castro, J., & Zamora, R. (2003). 'Pine processionary caterpillar Thaumetopoea pityocampa as a new threat for relict Mediterranean Scots pine forests under climatic warming', *Biological Conservation*. DOI: 10.1016/S0006-3207(02)00183-0
Huang, H., Li, X., & Chen, C. (2018). 'Individual tree crown detection and delineation from very-high-resolution UAV images based on bias field and marker-controlled watershed segmentation

algorithms', *IEEE Journal of Selected Topics in Applied Earth Observations and Remote Sensing*. DOI: 10.1109/JSTARS.2018.2830410
Huang, Y., Li, J., & Fan, N. (2008). 'Image mosaicing for UAV application', *Proceedings - 2008 International Symposium on Knowledge Acquisition and Modeling, KAM 2008*, 663–7. IEEE. DOI: 10.1109/KAM.2008.73
Johnson, E. W., & Ross, J. (2008). 'Quantifying error in aerial survey data', *Australian Forestry*. DOI: 10.1080/00049158.2008.10675038
Johnson, J., & Jacob, M. (2010). *Monitoring the effects of air pollution on forest condition in Europe: Is crown defoliation an adequate indicator?*. *IForest*, Vol. 3. DOI: 10.3832/ifor0538-003
de Jong, W., Pokorny, B., Katila, P., Galloway, G., & Pacheco, P. (2018). 'Community forestry and the sustainable development goals: A two way street', *Forests*, 9/6: 1–18. DOI: 10.3390/f9060331
Jonikavičius, D., & Mozgeris, G. (2013). 'Rapid assessment of wind storm-caused forest damage using satellite images and stand-wise forest inventory data', *IForest*, 6/1: 150–5. DOI: 10.3832/ifor0715-006
Kamdi, S., & Krishna, R. K. (2012). 'Image Segmentation and Region Growing Algorithm', *International Journal of Computer Technology and Electronics Engineering*. DOI: 10.4028/www.scientific.net/AMR.706-708.1799
Kazakis, G., Ghosn, D., Vogiatzakis, I. N., & Papanastasis, V. P. (2007). 'Vascular plant diversity and climate change in the alpine zone of the Lefka Ori, Crete', *Biodiversity and Conservation*, 16/6: 1603–15. DOI: 10.1007/s10531-006-9021-1
Ke, Y., Quackenbush, L. J., Resources, E., & Engineering, F. (2008). 'COMPARISON OF INDIVIDUAL TREE CROWN DETECTION AND DELINEATION',.
Kim, M., Madden, M., & Warner, T. (2008). 'Capítulo 3.2 Estimation of optimal image object size for the segmentation of forest stands with multispectral IKONOS imagery'. *Object-Based Image Analysis: Spatial Concepts for Knowledge-Driven Remote Sensing Applications*, pp. 291–307. DOI: 10.1007/978-3-540-77058-9_16
Knippers, R., & Tempfli, K. (2013). 'Spatial referencing and satellite-based positioning'. *The Core of GIScience: a systems basted approach*. DOI: 10.1098/rspb.2008.0457
Landgrebe, D. A. (2005). *Signal theory methods in multispectral remote sensing.*, Vol. 29. John Wiley & Sons.
Lang, S., Tiede, D., & Developer, D. (2007). 'Definiens Developer'. *GIS Business 9*. DOI: 10.1586/14737167.2.4.337
Lausch, A., Erasmi, S., King, D. J., Magdon, P., & Heurich, M. (2017). 'Understanding forest health with Remote sensing-Part II-A review of approaches and data models', *Remote Sensing*, 9/2: 1–33. DOI: 10.3390/rs9020129
Leckie, D. G., Jay, C., Gougeon, F. A., Sturrock, R. N., & Paradine, D. (2004). 'Detection and assessment of trees with Phellinus weirii (laminated root rot) using high resolution multi-spectral imagery', *International Journal of Remote Sensing*. DOI: 10.1080/0143116031000139926
Lehmann, J. R. K., Nieberding, F., Prinz, T., & Knoth, C. (2015). 'Analysis of unmanned aerial system-based CIR images in forestry-a new perspective to monitor pest infestation levels', *Forests*, 6/3: 594–612. DOI: 10.3390/f6030594
Liu, D., & Xia, F. (2010). 'Assessing object-based classification: Advantages and limitations', *Remote Sensing Letters*. DOI: 10.1080/01431161003743173
Lyons, M. B., Keith, D. A., Phinn, S. R., Mason, T. J., & Elith, J. (2018). 'A comparison of resampling methods for remote sensing classification and accuracy assessment', *Remote Sensing of Environment*. DOI: 10.1016/j.rse.2018.02.026
Meigs, G. W., Kennedy, R. E., & Cohen, W. B. (2011). 'A Landsat time series approach to characterize bark beetle and defoliator impacts on tree mortality and surface fuels in conifer forests', *Remote Sensing of Environment*. DOI: 10.1016/j.rse.2011.09.009
Mendel, Z., & Schiller, G. (1993). 'Biogeography of Matsucoccus josephi Bodenheimer et Harpaz in Crete and mainland Greece', *Annales des Sciences Forestieres*. DOI: 10.1051/forest:19930405
Meng, J., Li, S., Wang, W., Liu, Q., Xie, S., & Ma, W. (2016). 'Mapping forest health using spectral and textural information extracted from SPOT-5 satellite images', *Remote Sensing*. DOI: 10.3390/rs8090719
Minařík, R., & Langhammer, J. (2016). 'Use of a multispectral UAV photogrammetry for detection and tracking of forest disturbance dynamics', *International Archives of the Photogrammetry, Remote Sensing and Spatial Information Sciences - ISPRS Archives*, 41: 711–8. DOI: 10.5194/isprsarchives-

XLI-B8-711-2016
Mita, E., Tsitsimpikou, C., Tsiveleka, L., Petrakis, P. V., Ortiz, A., Vagias, C., & Roussis, V. (2002). 'Seasonal variation of oleoresin terpenoids from Pinus halepensis and Pinus pinea and host selection of the scale insect Marchalina hellenica (homoptera, coccoidea, margarodidae, coelostonidiinae)', *Holzforschung*. DOI: 10.1515/HF.2002.087
Mohan, M., Silva, C. A., Klauberg, C., Jat, P., Catts, G., Hudak, A. T., & Dia, M. (2017). 'Individual Tree Detection from Unmanned Aerial Vehicle (UAV) Derived Canopy Height Model in an Open Canopy Mixed Conifer Forest', 1–17. DOI: 10.3390/f8090340
Möller, M., Lymburner, L., & Volk, M. (2007). 'The comparison index: A tool for assessing the accuracy of image segmentation', *International Journal of Applied Earth Observation and Geoinformation*, 9/3: 311–21. DOI: 10.1016/j.jag.2006.10.002
Näsi, R., Honkavaara, E., Blomqvist, M., Lyytikäinen-saarenmaa, P., Hakala, T., Viljanen, N., Kantola, T., et al. (2018). 'Urban Forestry & Urban Greening Remote sensing of bark beetle damage in urban forests at individual tree level using a novel hyperspectral camera from UAV and aircraft', *Urban Forestry & Urban Greening*, 30/December 2016: 72–83. Elsevier. DOI: 10.1016/j.ufug.2018.01.010
Näsi, R., Honkavaara, E., Lyytikäinen-Saarenmaa, P., Blomqvist, M., Litkey, P., Hakala, T., Viljanen, N., et al. (2015). 'Using UAV-based photogrammetry and hyperspectral imaging for mapping bark beetle damage at tree-level', *Remote Sensing*. DOI: 10.3390/rs71115467
NatureCconservancy. (2017). 'What Can Birds Tell Us About Forest Health? | The Nature Conservancy'. Retrieved July 13, 2018, from <https://www.nature.org/ourinitiatives/regions/northamerica/unitedstates/wisconsin/science/what-can-birds-tell-us-about-forest-health.xml>
Pekkarinen, A. (2004). *Image segmentation in multi- source forest inventory. Evaluation*.
Poona, N. K., & Ismail, R. (2013). 'Discriminating the occurrence of pitch canker fungus in Pinus radiata trees using QuickBird imagery and artificial neural networks', *Southern Forests*, 75/1: 29–40. DOI: 10.2989/20702620.2012.748255
Pscheidt, J. W., & Deangelis, J. D. (2004). 'Diseases and Insects', *Water*, March: 145–62.
Qi, J., Chehbouni, A., Huete, A. R., Kerr, Y. H., & Sorooshian, S. (1994). 'A modified soil adjusted vegetation index', *Remote Sensing of Environment*. DOI: 10.1016/0034-4257(94)90134-1
Raj, K. J., & Sivasathya, S. (2014). 'SVM and random forest classification of satellite image with NDVI as an additional attribute to the dataset'. *Advances in Intelligent Systems and Computing*. DOI: 10.1007/978-81-322-1771-8_9
Sankaran, S., Mishra, A., Ehsani, R., & Davis, C. (2010). 'A review of advanced techniques for detecting plant diseases'. *Computers and Electronics in Agriculture*. DOI: 10.1016/j.compag.2010.02.007
Sims, D. A., & Gamon, J. A. (2002). 'Relationships between leaf pigment content and spectral reflectance across a wide range of species, leaf structures and developmental stages', *Remote Sensing of Environment*. DOI: 10.1016/S0034-4257(02)00010-X
Skrzypietz, B. T. (2012). 'Unmanned Aircraft Systems for Civilian Missions', *Brandenburg Institute for Society and Security Policy Paper*. DOI: https://doi.org/10.1162/003465304323023778
Stephens, D., & Diesing, M. (2014). 'A comparison of supervised classification methods for the prediction of substrate type using multibeam acoustic and legacy grain-size data', *PLoS ONE*. DOI: 10.1371/journal.pone.0093950
Stone, C., Penman, T., & Turner, R. (2012). 'Managing drought-induced mortality in Pinus radiata plantations under climate change conditions: A local approach using digital camera data', *Forest Ecology and Management*. DOI: 10.1016/j.foreco.2011.10.008
Tang, L., & Shao, G. (2015). 'Drone remote sensing for forestry research and practices', *Journal of Forestry Research*, 26/4: 791–7. Northeast Forestry University. DOI: 10.1007/s11676-015-0088-y
Tolpekin, V. A., & Stein, A. (2013). 'The core of GIScience a systems-based approach', *The Core of GIScience*. DOI: 10.1016/B978-0-12-385889-4.00013-2
Tuominen, J., Lipping, T., Kuosmanen, V., & Haapane, R. (2009a). 'Remote Sensing of Forest Health', *Geoscience and Remote Sensing*, October. DOI: 10.5772/8283
——. (2009b). 'Remote Sensing of Forest Health', *Geoscience and Remote Sensing*, May 2014. DOI: 10.5772/8283
——. (2009c). 'Remote Sensing of Forest Health'. *Geoscience and Remote Sensing*. DOI: 10.5772/8283
Viera, A. J., & Garrett, J. M. (2005). 'Understanding interobserver agreement: The kappa statistic', *Family Medicine*. DOI: Vol. 37, No. 5
Wang, J., Sammis, T. W., Gutschick, V. P., Gebremichael, M., Dennis, S. O., & Harrison, R. E. (2010).

'Review of Satellite Remote Sensing Use in Forest Health Studies~!2010-01-27~!2010-04-05~!2010-06-29~!', *The Open Geography Journal*, 3/1: 28–42. DOI: 10.2174/1874923201003010028

Wang, L., Gong, P., & Biging, G. S. (2004). 'Individual Tree-Crown Delineation and Treetop Detection in High-Spatial-Resolution Aerial Imagery', *Photogrammetric Engineering & Remote Sensing*. DOI: 10.14358/PERS.70.3.351

Wulder, M. A., Dymond, C. C., White, J. C., Leckie, D. G., & Carroll, A. L. (2006). 'Surveying mountain pine beetle damage of forests: A review of remote sensing opportunities'. *Forest Ecology and Management*. DOI: 10.1016/j.foreco.2005.09.021

Wulder, M. A., White, J. C., Bentz, B. J., & Ebata, T. (2006). 'Augmenting the existing survey hierarchy for mountain pine beetle red-attack damage with satellite remotely sensed data1'. *Forestry Chronicle*. DOI: 10.5558/tfc82187-2

Xiao, Q., & McPherson, E. G. (2005). 'Tree health mapping with multispectral remote sensing data at UC Davis, California', *Urban Ecosystems*. DOI: 10.1007/s11252-005-4867-7

Xu, Y., Ou, J., He, H., Zhang, X., & Mills, J. (2016). 'Mosaicking of Unmanned Aerial Vehicle imagery in the absence of camera poses', *Remote Sensing*, 8/3. DOI: 10.3390/rs8030204

Zhang, Y. J. (1996). 'A survey on evaluation methods for image segmentation', *Pattern Recognition*. DOI: 10.1016/0031-3203(95)00169-7

APPENDICES

Appendix1: PIX4d software quality check report site 1

Project	site1final
Processed	2018-09-28 21:12:32
Camera Model Name(s)	Sequoia_4.0_1280x960 (Green), Sequoia_4.0_1280x960 (Red), Sequoia_4.0_1280x960 (Red edge), Sequoia_4.0_1280x960 (NIR)
Rig name(s)	«Sequoia»
Average Ground Sampling Distance (GSD)	8.55 cm / 3.37 in
Area Covered	0.445 km^2 / 44.5415 ha / 0.17 sq. mi. / 110.1214 acres
Time for Initial Processing (without report)	52m:18s

Quality Check

Images	median of 10000 keypoints per image	✓
Dataset	1288 out of 1360 images calibrated (94%), all images enabled	⚠
Camera Optimization	0.01% relative difference between initial and optimized internal camera parameters	✓
Matching	median of 2727.84 matches per calibrated image	✓
Georeferencing	yes, no 3D GCP	⚠

Appendix2: PIX4d software quality check report site

Project	site2final
Processed	2018-09-28 18:49:43
Camera Model Name(s)	Sequoia_4.0_1280x960 (Green), Sequoia_4.0_1280x960 (Red), Sequoia_4.0_1280x960 (Red edge), Sequoia_4.0_1280x960 (NIR)
Rig name(s)	«Sequoia»
Average Ground Sampling Distance (GSD)	8.43 cm / 3.32 in
Area Covered	0.363 km^2 / 36.3346 ha / 0.14 sq. mi. / 89.8311 acres
Time for Initial Processing (without report)	16m:33s

Quality Check

Images	median of 10000 keypoints per image	✓
Dataset	924 out of 980 images calibrated (94%), all images enabled	⚠
Camera Optimization	0.02% relative difference between initial and optimized internal camera parameters	✓
Matching	median of 3305.24 matches per calibrated image	✓
Georeferencing	yes, no 3D GCP	⚠

Appendix 3: ANOVA test within the NDRE in site 1

mean					
	Sum of Squares	**df**	**Mean Square**	**F**	**Sig.**
Between Groups	0.114	2	0.057	10.966	4.41E-05
Within Groups	0.593	114	0.005		
Total	0.707	116			

Appendix 4:Post hoc test within the NDRE in site 1

(I) class		**Mean Difference (I-J)**	**Std. Error**	**Sig.**	**95% Confidence Interval**	
					Lower Bound	Upper Bound
heathy	moderate	0.0396	0.016	0.04426	0.001	0.078
	severe	0.0765	0.0163	0.00002	0.038	0.115
moderate	heathy	-0.0396	0.0163	0.04426	-0.078	-0.001
	severe	0.0369	0.0163	0.06604	-0.002	0.076
severe	heathy	-0.0765	0.0163	0.00002	-0.115	-0.038
	moderate	-0.0369	0.0163	0.06604	-0.076	0.002
*. The mean difference is significant at the 0.05 level.						

Appendix 5:ANOVA test within the NDVI in site1

mean					
	Sum of Squares	**df**	**Mean Square**	**F**	**Sig.**
Between Groups	0.411	2	0.205	12.663	1.081E-05
Within Groups	1.848	114	0.016		
Total	2.259	116			

Appendix 6 Post hoc test within the NDVI in site 1

(I) class		Mean Difference (I-J)	Std. Error	Sig.	95% Confidence Interval	
					Lower Bound	Upper Bound
healthy	moderate	0.0758	0.0288	0.026	0.0074	0.1443
	severe	0.1451	0.0288	5.475E-06	0.0766	0.2135
moderate	healthy	-0.0758	0.0288	0.026	-0.1443	-0.0074
	severe	0.0692	0.0288	0.047	0.0008	0.1377
severe	healthy	-0.1451	0.0288	5.475E-06	-0.2135	-0.0766
	moderate	-0.0692	0.0288	0.047	-0.1377	-0.0008
*. The mean difference is significant at the 0.05 level.						

:

Appendix 7:ANOVA test within the SAVI in site 1

mean					
	Sum of Squares	**df**	**Mean Square**	**F**	**Sig.**
Between Groups	0.068	2	0.034	13.622	4.957E-06
Within Groups	0.284	114	0.002		
Total	0.352	116			

Appendix 8:Post hoc test within the SAVI in site 1

(I) class		**Mean Difference (I-J)**	**Std. Error**	**Sig.**	**95% Confidence Interval**	
					Lower Bound	**Upper Bound**
healthy	moderate	0.031	0.0113	0.017	0.0046	0.058
	severe	0.059	0.0113	2.473E-06	0.0321	0.086
moderate	healthy	-0.031	0.0113	0.017	-0.0583	-0.005
	severe	0.028	0.0113	0.043	0.0007	0.054
severe	healthy	-0.059	0.0113	2.473E-06	-0.0859	-0.032
	moderate	-0.028	0.0113	0.043	-0.0544	-0.001
*. The mean difference is significant at the 0.05 level.						

Appendix 9:ANOVA test within the NDRE in site 2

mean					
	Sum of Squares	**df**	**Mean Square**	**F**	**Sig.**
Between Groups	0.126	2	0.063	11.496	0.000
Within Groups	0.625	114	0.005		
Total	0.751	116			

Appendix 10:post hoc test within the NDRE in site 2

(I) class		**Mean Difference (I-J)**	**Std. Error**	**Sig.**	**95% Confidence Interval**	
					Lower Bound	**Upper Bound**
heathy	moderate	0.042	0.017	0.036	0.002	0.082
	severe	0.080	0.017	0.000	0.041	0.120
moderate	heathy	-0.042	0.017	0.036	-0.082	-0.002
	severe	0.038	0.017	0.062	-0.002	0.078
severe	heathy	-0.080	0.017	0.000	-0.120	-0.041
	moderate	-0.038	0.017	0.062	-0.078	0.002
*. The mean difference is significant at the 0.05 level.						

Appendix 11:ANOVA test within the NDVI in site 2

mean					
	Sum of Squares	**df**	**Mean Square**	**F**	**Sig.**
Between Groups	0.321	2	0.160	13.038	0.000
Within Groups	1.180	96	0.012		
Total	1.501	98			

.

Appendix 12:Post hoc test within the NDVI in site 2

(I) class		**Mean Difference (I-J)**	**Std. Error**	**Sig.**	**95% Confidence Interval**	
					Lower Bound	**Upper Bound**
healthy	moderate	0.072	0.027	0.027	0.007	0.136
	severe	0.072	0.027	0.000	0.074	0.204
moderate	healthy	0.072	0.027	0.027	-0.136	-0.007
	severe	0.072	0.027	0.039	0.003	0.133
severe	healthy	0.072	0.027	0.000	-0.204	-0.074
	moderate	0.072	0.027	0.039	-0.133	-0.003
*. The mean difference is significant at the 0.05 level.						

Appendix 13:ANOVA test within the SAVI in site 2

mean					
	Sum of Squares	**df**	**Mean Square**	**F**	**Sig.**
Between Groups	0.086	2	0.043	15.409	0.000
Within Groups	0.268	96	0.003		
Total	0.354	98			

Appendix 14:Post hoc test within the SAVI in site 2

(I) class		**Mean Difference (I-J)**	**Std. Error**	**Sig.**	**95% Confidence Interval**	
					Lower Bound	Upper Bound
healthy	moderate	0.039	0.013	0.010	0.008	0.070
	severe	0.072	0.013	0.000	0.041	0.103
moderate	healthy	-0.039	0.013	0.010	-0.070	-0.008
	severe	0.033	0.013	0.032	0.002	0.064
severe	healthy	-0.072	0.013	0.000	-0.103	-0.041
	moderate	-0.033	0.013	0.032	-0.064	-0.002
***. The mean difference is significant at the 0.05 level.**						

SITE 1: CLASSIFICATION ERROR MATRIX

Appendix 15:Site1 Error matrix of classification NDVI Using Random forest classifier

NDVI	Severe	Moderate	Healthy	Sum
Severe	7	2	0	9
Moderate	4	9	1	14
Healthy	0	1	9	10
Sum	11	12	10	
Producer	0.64	0.75	0.90	
User	0.78	0.64	0.90	
Overall Accuracy	0.76			
KIA	0.63			

Appendix 16:Site1 Error matrix of NDVI combined Using SVM

NDVI	severe	Moderate	Healthy	Sum
Severe	8	3	0	11
Moderate	3	8	2	13
Healthy	0	1	8	9
Sum	11	12	10	
Producer	0.73	0.67	0.80	
User	0.73	0.62	0.89	
Overall Accuracy	0.73			
KIA	0.59			

Appendix 17:Site1 Error matrix of NDRE combined Using Random forest classifier

NDRE	Severe	Moderate	Healthy	Sum
Severe	3	0	0	3
Hoderate	8	10	1	19
Healthy	0	2	9	11
Sum	11	12	10	
Producer	0.27	0.83	0.90	
User	1.00	0.53	0.82	
Overall Accuracy	0.66			
KIA	0.49			

Appendix 18:Site1 Error matrix of NDRE Using SVM

NDRE	severe	moderate	healthy	Sum
Severe	3	0	0	3
Moderate	8	10	2	20
Healthy	0	2	8	10
Sum	11	12	10	
Producer	0.27	0.83	0.80	
User	1.00	0.50	0.80	
Overall Accuracy	0.64			
KIA	0.43			

Appendix 19:Site2 Error matrix of SAVI Using Random forest classifier

SAVI	Severe	Moderate	Healthy	Sum
Severe	9	2	0	11
Soderate	2	9	2	13
Healthy	0	1	8	9
Sum	11	12	10	
Producer	0.82	0.75	0.80	
User	0.82	0.69	0.89	
Overall Accuracy	0.79			
KIA	0.68			

Appendix 20:Site1 Error matrix of SAVI Using SVM classifier

SAVI	Severe	Moderate	Healthy	Sum	
Severe	7	1	0	8	
Moderate	4	10	2	16	
Healthy	0	1	8	9	
Sum	11	12	10		
Producer	0.64	0.83	0.80		
User	0.88	0.63	0.89		
Overall Accuracy	0.77				
KIA	0.63				

Appendix 21:Site1 Error matrix of classification all vegetation indices combined Using Random forest classifier

COMBINED VI	severe	moderate	healthy	Sum
severe	9	1	0	10
moderate	2	10	1	13
healthy	0	1	9	10
Sum	11	12	10	
Producer	0.82	0.83	0.90	
User	0.90	0.77	0.90	
Overall Accuracy	0.85			
KIA	0.77			

Appendix 22:Site1 Error matrix of classification all vegetation indices combined Using SVM

	severe	moderate	healthy	Sum
severe	8	1	0	9
moderate	3	10	1	14
healthy	0	1	9	10
Sum	11	12	10	
Producer	0.73	0.83	0.90	
User	0.89	0.71	0.90	
Overall Accuracy	0.82			
KIA	0.73			

SITE TWO: CLASSIFICATION ERROR MATRIX

Appendix 23:Site2 Error matrix of NDVI combined Using Random forest classifier

User Class \ Sample	Severe	Healthy	Moderate	Sum
Severe	6	0	0	6
Healthy	0	7	1	8
Moderate	7	4	11	22
Sum	13	11	12	
Producer	0.46	0.64	0.92	
User	1.00	0.88	0.50	
Overall Accuracy	0.67			
KIA	0.50			

Appendix 24:Site2 Error matrix of NDVI combined Using SVM

User Class \ Sample	severe	Moderate	healthy	Sum
Severe	6	0	0	6
Healthy	0	6	1	7
Moderate	7	5	11	23
Sum	13	11	12	
Producer	0.46	0.55	0.92	
User	1.00	0.86	0.48	
Overall Accuracy	0.64			
KIA	0.46			

Appendix 25:Site2 Error matrix of NDRE Using Random forest classifier

User Class \ Sample	Severe	Moderate	Healthy	Sum
Severe	11	7	1	19
Moderate	1	2	1	4
Healthy	1	3	9	13
Sum	13	12	11	
Producer	0.85	0.17	0.82	
User	0.58	0.50	0.69	
Overall Accuracy	0.61			
KIA	0.41			

Appendix 26:Site2 Error matrix of NDRE Using SVM

User Class \ Sample	Severe	Moderate	Healthy	Sum
Severe	11	8	1	20
Moderate	1	1	1	3
Healthy	1	3	9	13
Sum	13	12	11	
Producer	0.85	0.08	0.82	
User	0.55	0.33	0.69	
Overall Accuracy	0.58			
KIA	0.37			

Appendix 27:Site2 Error matrix of SAVI Using Random forest classifier

User Class \ Sample	Severe	Moderate	Healthy	Sum
Severe	11	5	1	17
Moderate	2	5	1	8
Healthy	0	2	9	11
Sum	13	12	11	
Producer	0.85	0.42	0.82	
User	0.65	0.63	0.82	
Overall Accuracy	0.70			
KIA	0.54			

Appendix 28:Site2 Error matrix of classification all vegetation indices combined Using Random forest classifier

User Class \ Sample	severe	moderate	healthy	Sum
severe	11	4	0	15
moderate	2	7	1	10
healthy	0	1	10	11
Sum	13	12	11	
Producer	0.85	0.58	0.91	
User	0.73	0.70	0.91	
Overall Accuracy	0.78			
KIA	0.67			

Appendix 29:Site2 Error matrix of classification all vegetation indices combined Using Random forest classifier

User Class \ Sample	Severe	Moderate	Healthy	Sum
Severe	11	4	1	16
Moderate	2	7	1	10
Healthy	0	1	9	10
Sum	13	12	11	
Producer	0.85	0.58	0.82	
User	0.69	0.70	0.90	
Overall Accuracy	0.75			
KIA	0.62			

Appendix 30: Fieldwork data collection form

Observation NO:	N:	E:	
Tree Health Status	healthy	moderate	severe
Defoliation status	0-10%	>10%-60%	>60%
Discoloration status	0-10%	>10%-60%	> 60%